Durham E-Theses

The separation of the particle and light fronts in cosmic ray showers at mountain altitudes

Stephenson, I.

How to cite:

Use policy

THE SEPARATION OF THE PARTICLE AND LIGHT FRONTS IN COSMIC RAY SHOWERS AT MOUNTAIN ALTITUDES

by

I. Stephenson, B.Sc.

A Thesis submitted to the University of Durham
in accordance with the Regulations for Admittance
to the Degree of Master of Science

Department of Physics
University of Durham

February, 1981

ABSTRACT

This Thesis describes a study of the time separation of the Cerenkov light and particle fronts in large $(10^{16} - 10^{18}$ eV) cosmic ray air showers at an atmospheric depth of 862 g cm^{-2}. The work formed only part of a much larger experiment conducted at the Dugway Proving Ground, Utah, U.S.A. during the autumn and winter months of 1977/8, 1978/79, 1979/80.

The aim of this particular work is to refine our understanding of the time delay between the Cerenkov light and the particle fronts, and to establish this time as a depth of maximum sensitive measure. Since this is a prime indicator of the mass of the initiating primary, the time delay which can be readily measured may yield a method of estimating the primary mass of energetic cosmic rays.

An account of earlier measurements of Cerenkov radiation is given as well as a theoretical treatment of the time separation based on computer simulations of showers. The experimental results are presented which demonstrate a sensitivity to cascade development and recommendations for future time separation studies are made.

C O N T E N T S

CONTENTS

CHAPTER I

INTRODUCTION

1.1 Historical

Cosmic rays have held the attention of experimenters for more than seventy years. It was in 1901 that Wilson noticed a residual ionization in his ionization chambers even in the absence of any local radioactive material. Since the ionization could not be eliminated by lead shielding, he hypothesised that the phenomena was likely to be due to a penetrating radiation of unknown origin.

In 1912 Hess flew detecting instruments to an altitude of 5 km using balloons. He discovered that the intensity of the radiation increased with altitude. From this he concluded that the radiation originated outside or in the upper atmosphere, but since the radiation persisted day and night, the Sun could not be the direct source and therefore the radiation must be of extra-terrestrial origin.

In the 1930's a hard and soft core was discovered. The hard core consisted of penetrating particles which today are known as muons. The soft core consisted of easily absorbed particles, now known to be electrons and photons. Balloon borne instruments showed that the cosmic ray intensity maximised at 12 km indicating that most of the particles must be produced in the atmosphere thus demonstrating the secondary nature of cosmic rays within the atmosphere.

In the 1940's, pions and muons were discovered from tracks in photographic emulsions. Since these were created in high energy nuclear collisions, the missing link necessary to account for the large flux of electrons and photons in extensive air showers had been found.

In the 1950's satellites made possible the investigation of cosmic radiation free from terrestrial influences and there followed the
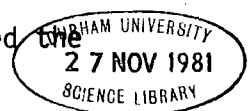
discovery of the Van Allen Belts, the solar wind and interplanetary magnetic fields, all phenomena closely associated with cosmic ray research below a primary energy of about 10^{12} eV.

1.2 The cosmic ray energy spectrum

One striking feature of the cosmic ray energy distribution is the similarity of the energy distribution of all nuclear components, suggesting an acceleration mechanism that does not discriminate between them.

Figure 1.1 shows the energy spectrum which in fact extends over at least thirteen decades of energy. The change of slope at $\sim 3 \times 10^{15}$ eV has one explanation by considering a proton with that energy. If a uniform galactic magnetic field is assumed then the radius of curvature of the proton is comparable with the thickness of the galactic disc (~ 400 light years). It would therefore be expected that particles of lower charge would preferentially diffuse out of the Galaxy, enriching the beam with heavier nuclei at 10^{16} to 10^{18} eV. If particles of these higher energies originated from the Galaxy more of them would appear to come from the galactic centre; however, an isotropic distribution of incidence is observed which forces the acceptance of the notion that very high energy cosmic rays ($Ep > 10^{18}$ eV) are of extragalactic origin.

The acceleration of particles to high energies so difficult on Earth, appears to occur readily and frequently in some astronomical environments. The distribution of energy in galactic cosmic rays contains information about the acceleration mechanisms although all directional information is lost due to the particles' interaction with the galactic, solar and terrestrial magnetic fields. This is confirmed by the isotropic arrival directions of cosmic rays ($Ep \gtrsim 10^{18}$ eV).
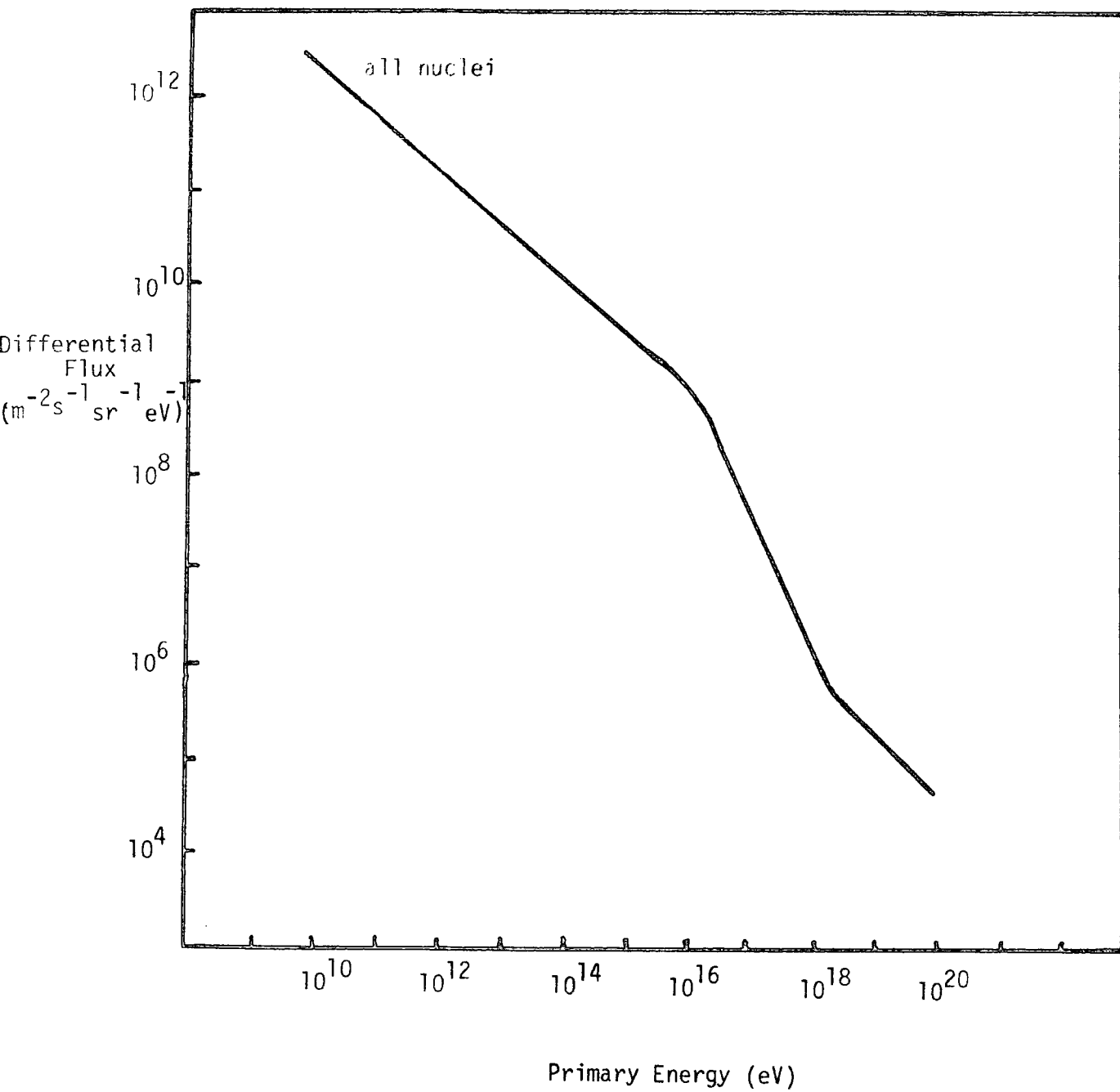
Figure 1.1   The Cosmic Ray Energy Spectrum.

1.3 The cosmic ray mass spectrum

Table 1 shows the results of direct measurements of the relative abundance of protons and neutrons, helium nuclei and heavier particles at various low energies.

The mass spectrum at 150 MeV/nucleon exhibits some striking features, see Figure 1.2. It greatly resembles the estimated cosmic abundance distribution of the elements indicating that cosmic rays originate from objects containing the element distribution consistent with evolution through thermonuclear processes. Figure 1.2 also shows a relatively high abundance of the elements lithium, beryllium and boron which are practically absent in stellar objects. These elements must therefore have been produced in inter-stellar space and there exists good evidence that they are the product of collisions and subsequent spallation mostly of carbon and oxygen with particles present in the tenuous inter-stellar gas. Their abundance has led to the estimate that cosmic rays on average encounter 3 to 5 g cm^{-2} of interstellar matter. If this is so and the density of interstellar matter is one or two hydrogen atoms per cm^3, then it can be deduced that the dwelling time of a cosmic ray particle in the galaxy is about 10^6 years.

Until 1967 no nucleus heavier than iron was known to exist in cosmic radiation. The discovery in meteoritic crystals of particle tracks produced by primaries heavier than iron and subsequent observation of cosmic rays of higher nuclear charge changed this situation. The frequency of these heavy nuclei is extremely low, for each nucleus with a charge in excess of 31, 10^4 nuclei in the iron group (charge around 26) are found.

1.4 Extensive Air Showers

A particle with an energy greater than 10^{16} eV has an extremely low flux i.e. 1/m^2/2 years at 10^{16} eV, 1/m^3/3000 years at 10^{18} eV

TABLE 1

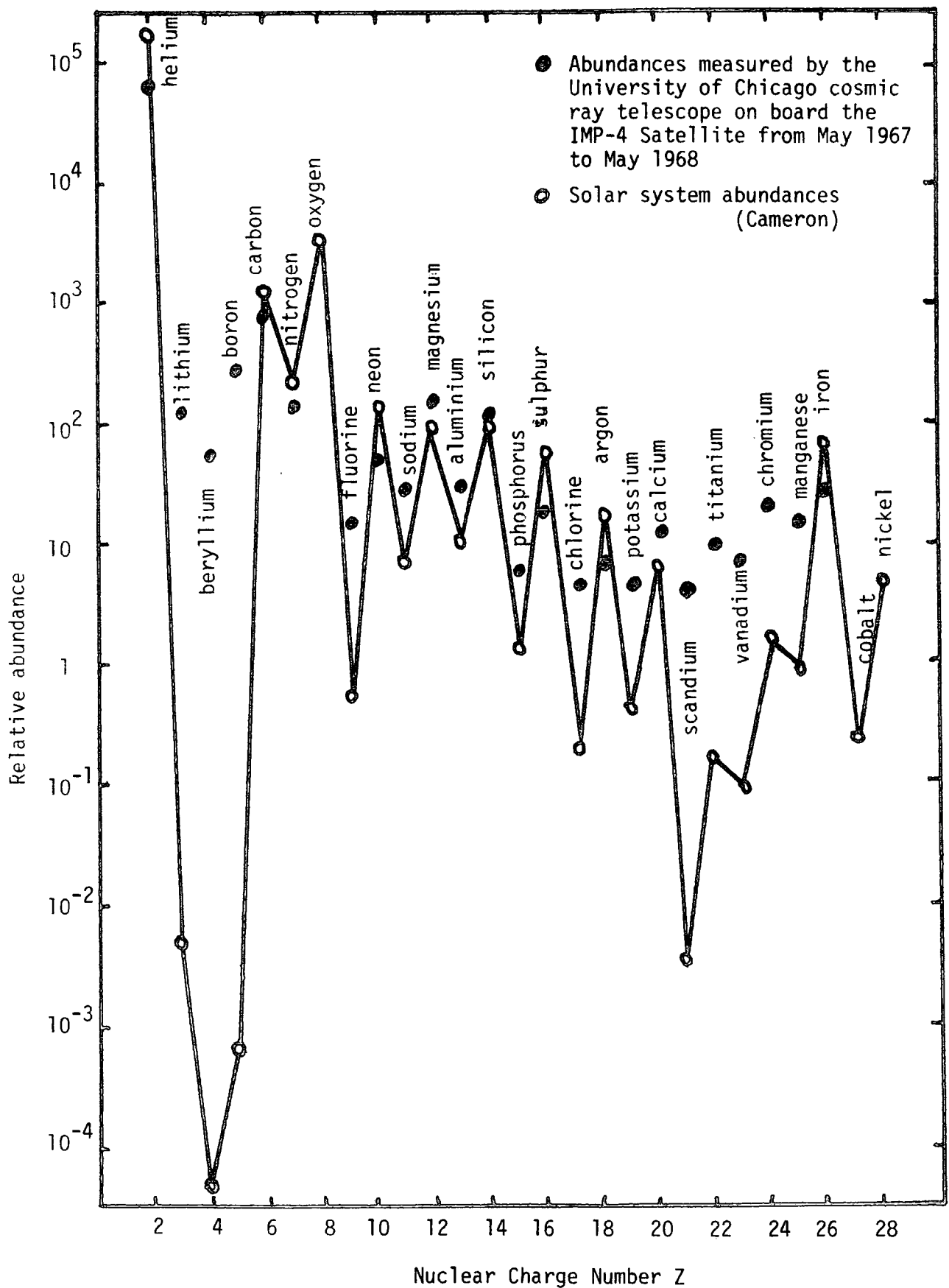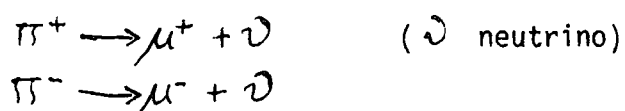| Energy (eV)	Total No. of Events	% Protons & Neutrons	% of Alpha Particles	% of heavier Particles	Reference
3.7×10^{11}	46	80	13	7	Malhotra et al.,(1966)
$>10^{12}$	112	46	16	38	McCusker (1967)
Universal composition	-	~ 99	< 1	< 0.02	-

Figure 1.2   The cosmic ray mass spectrum at 150 MeV/nucleon.

and $1/m^2/5 \times 10^5$ years at 10^{19} eV. It is, therefore, impossible to observe the primary beam directly. However, the atmosphere presents itself as an absorber of thickness 1030 g cm^{-2}, which is large when compared to the mean free path of a proton. The primary will therefore interact with air nuclei several times before reaching ground level. Each interaction produces secondary particles which may also interact further and will produce secondaries which can be detected over a wide range at ground level. Not all the particles in the extensive air shower (EAS) proceed in the same direction, although there is a core around which most are clustered. Particles in single air showers have been detected more than 1000 m apart. The majority however land in an area of 70 m radius (at sea level) and within about 10^{-7} s of each other in time.

Figure 1.3 shows diagramatically a primary/air nucleus interaction and all the secondaries that may be produced. After interaction the majority of secondary particles are pions. The primary will then continue with approximately half its initial energy. Neutral pions (π^0) decay almost instantaneously $(t_{\frac{1}{2}} = 10^{-16}s)$ to two photons which travel on average 48 g cm^{-2} before undergoing pair production. The positron and electron thus produced generate new photons along their paths by radiation as they pass near nuclei. These photons also initiate pair production which in turn results in more photons. Thus the electron-photon cascade develops. The average energy of the particle decreases as the particle number grows. The positive and negative pions (π^+, π^-) produced in the interaction may be travelling sufficiently fast for the relativistic time dilation effect to allow them a life time long enough to interact with other air nuclei, thus producing more pions. Unless this occurs the pions will decay to muons.

$$\pi^+ \longrightarrow \mu^+ + \nu \qquad (\nu \text{ neutrino})$$
$$\pi^- \longrightarrow \mu^- + \nu$$

Primary Particle

"Strong" nuclear interaction
with an air nucleus

Knock on
nucleons

Kaons
Hyperons

Nuclear
interac-
tion

Pions

π^+ π^- π^o

Decay

Photoproduction

Nuclear Interaction

Decay

Decay

ν μ

γ

Decay

Pair production
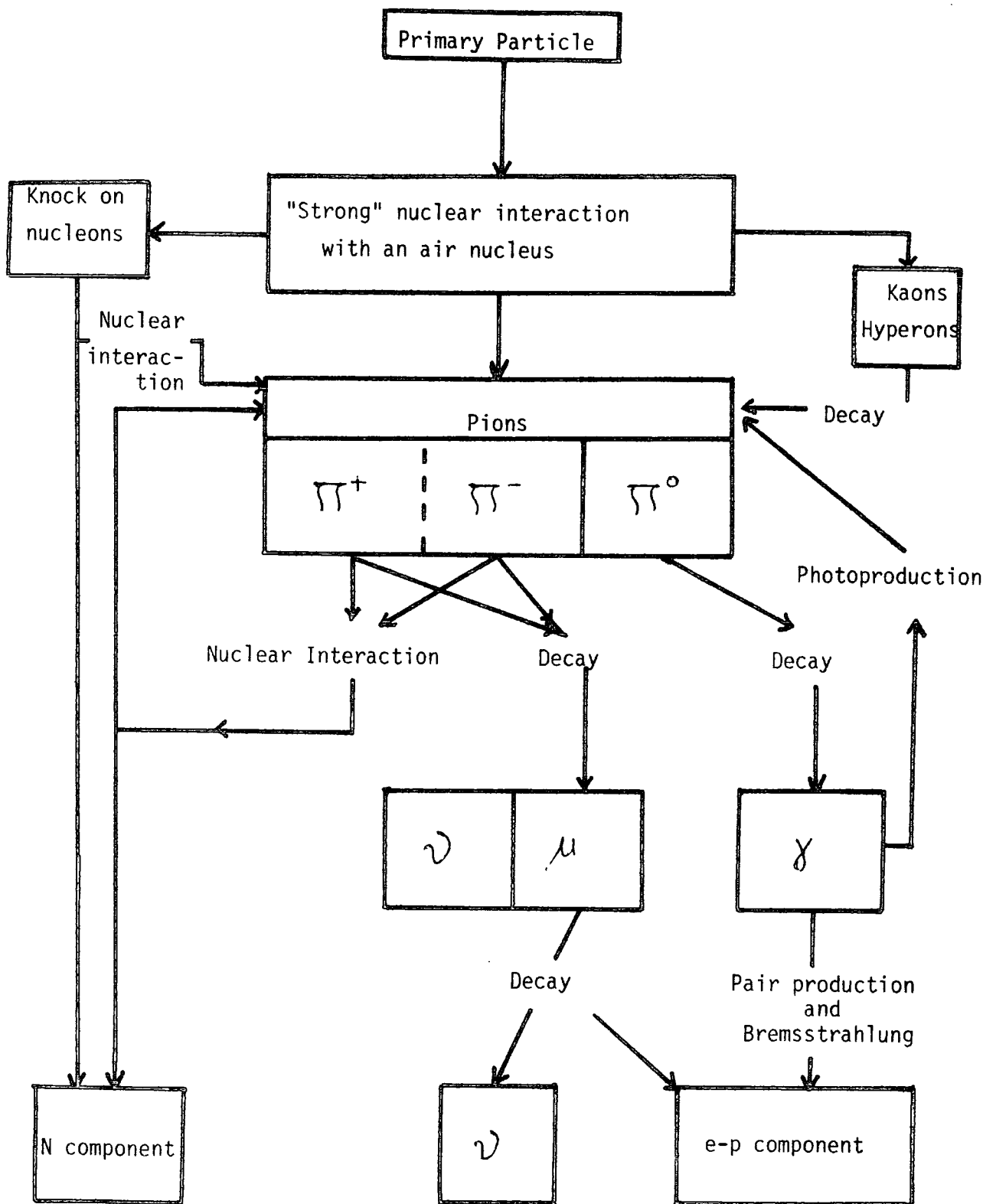and
Bremsstrahlung

N component

ν

e-p component

Figure 1.3   Diagramatical representation of a primary/air nucleus
interaction and the resulting secondaries

Muons retain about 80% of the energy of the pions and very seldom lose it by nuclear collision. Instead there is a gradual loss of energy by ionization. Many muons decay during flight through the atmosphere. About two thirds of the energy and momentum of such a muon is taken away by neutrinos and the rest by a high energy electron or positron.

$$\mu^+ \longrightarrow e^+ + \overline{\nu} + \nu$$
$$\mu^- \longrightarrow e^- + \overline{\nu} + \nu$$
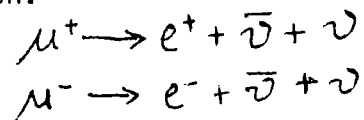
Most muons of several GeV energies survive to reach ground level where they can penetrate up to 35 m of earth.

Following the initial interaction a cascade will build up and as the primary continues the cascade will be continually replenished. The electromagnetic cascade is the largest but it only contains 10% of the total energy, the most energetic is the hadronic cascade. Since the electrons and muons have a wide lateral spread, sampling their flux at various core distances at ground level will give information about the cascade and hence the energy, mass and arrival direction of the primary.

1.5 The present work

This thesis discusses measurements of Cerenkov radiation in large ($\sim 10^{17}$ eV) extensive air showers with particular reference to the time delay between the particle and Cerenkov light fronts.

The measurement of the time delay is presented as a technique which can be developed as a means of estimating the cascade development of an EAS and in turn, the primary mass. Particle density measurements are presented which show potential as being a measure of the cascade development.

CHAPTER II

CERENKOV RADIATION

2.1 Introduction

Coherent radiation is produced by the passage of relativistic particles through densemedia and was first detected by Cerenkov (1934). A classical explanation for the phenomenon was given by Frank and Tamm (1937) based on the electromagnetic theory.

The charged particle polarizes the medium in the region of the track and the depolarization results in the emission of Cerenkov light. In a simplified picture, spherical wavelets of light are emitted from the track of a relativistic particle. If the particle velocity, v, is less than the phase velocity of light, $^c/n$ (where n is the refractive index of the medium) then destructive interference of any radiated wavelets will occur. If $v > ^c/n$ then the wavelets from the particle track will interfere constructively and produce a conical wavefront travelling at an angle of θ to the particle track, as shown in the Huygens construction in Figure 2.1. Also shown in the figure is the constructionfor $v < ^c/n$ and the limiting case $v = ^c/n$.

From simple arguments, the Cerenkov Relation is obtained

$$\cos\theta = \frac{^c/n}{v} = (\beta n)^{-1}$$

2.2 Early measurements of Cerenkov radiation from the atmosphere.

In 1948, Blackett suggested that cosmic ray particles could produce Cerenkov radiation in the atmosphere, contributing about 0.01% of the night sky brightness.

In 1953 Jelley and Galbraith suggested that during an extensive air shower (EAS) there would be sufficient electrons radiating over a short period of time (10's of nanoseconds) to produce a Cerenkov photon density that would exceed the night sky background. In their experiment to verify this, they used a photomultiplier, with a suitably short time constant, at the focus of a vertically looking mirror ringed

$$v < {}^c/n$$

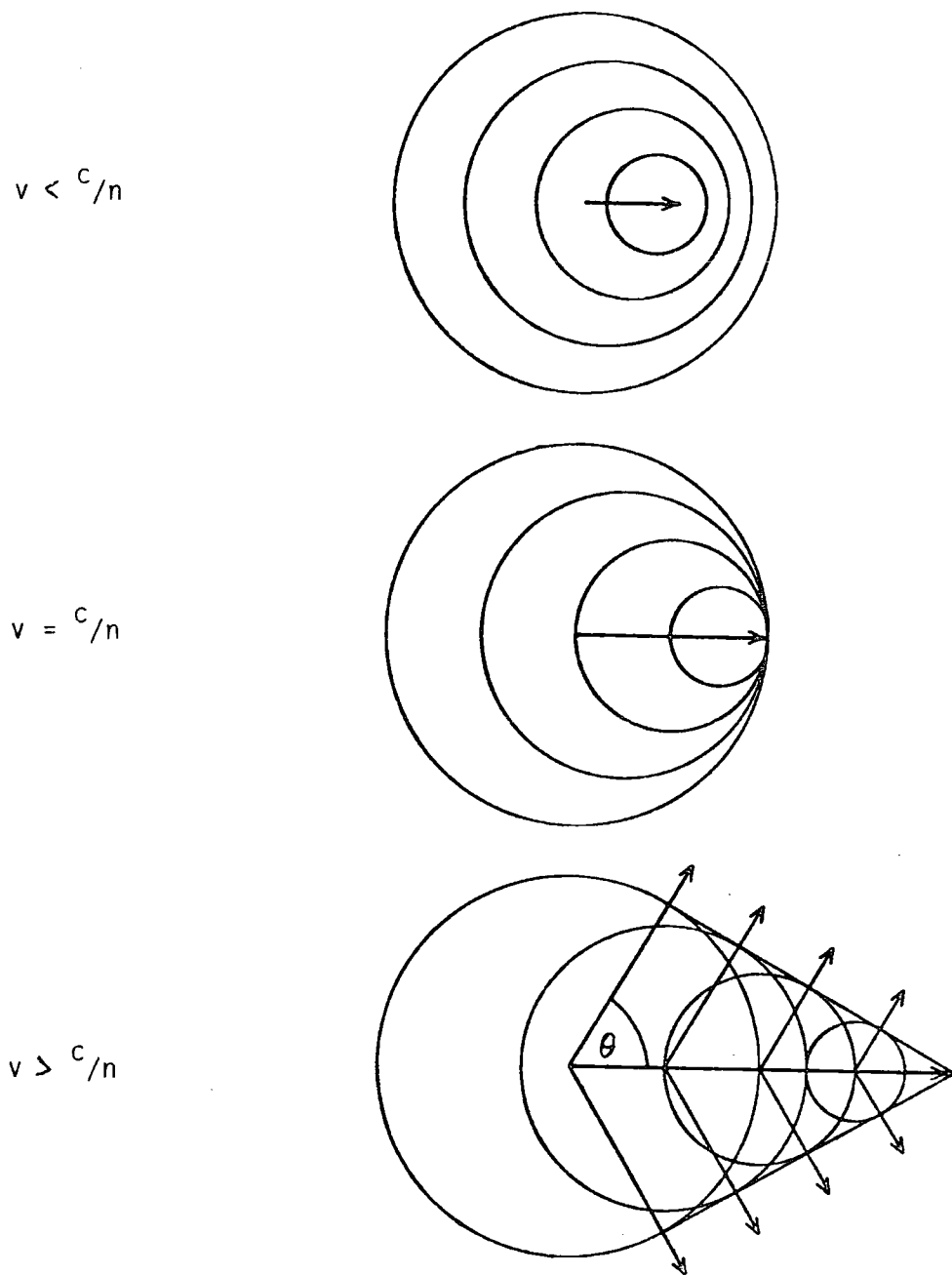$$v = {}^c/n$$

$$v > {}^c/n$$

θ

Figure 2.1 The Huygen's construction for Cerenkov Light from a particle with velocity v in a medium of refractive index n

by Geiger-Muller tubes and noted a co-incidence on 22 out of 50 occasions between the photomultiplier signal and the discharge of one or two Geiger-Muller tubes. Out of 19 three fold Geiger-Muller tube responses there were no photomultiplier signals. The 60 - 1 ratio in the size of the collection cones could account for this ($\sim 2\pi$ and 0.1 sr). They suggested that the recorded Cerenkov radiation might be produced in EAS having 10^5 - 10^6 electrons initiated by the more energetic cosmic rays ($\sim 10^{15}$ eV).

Later work by the same authors in 1955 at the Pic du Midi Observatory (altitude 2860 m) extended the investigation of the radiation and showed it to be polarized and having a spectrum rich in blue light and consistent with Cerenkov radiation.

Theoretical Considerations

Cerenkov radiation is not the only light emitted during the propogation of an EAS through the atmosphere, so it is necessary to consider why the light detected is that produced by the Cerenkov effect rather than other mechanisms. From Frank and Tamm (1937) the loss of energy E per unit path length by a particle of charge z and velocity β to Cerenkov radiation of wavelength λ between λ and $d\lambda$ is

$$\frac{dE}{dh} = 4\pi^2 z^2 \int \left(1 - \frac{1}{\beta^2 n^2}\right) \frac{d\lambda}{\lambda^3} \qquad \text{Equation 2.1}$$

Now n - 1 = 0.00029 at sea level and varies by approximately 2.5% over the visible spectrum from 400 nm to 700 nm; it is thus frequently taken as constant. For high energy electrons this expression reduces to:

$$\frac{dE}{dh} = 3.8\mu \times 10^{-14} \text{ Jm}^{-1}$$

where μ = n - 1. Assuming no variation in μ with altitude this reduces to 8.2 x 10^3 photons/radiation length (Boley 1964). Since, for electrons reaching sea level there are approximately 30 radiation lengths, one such electron would produce approximately 2.5 x 10^5 photons in total.

This calculation is an over-estimation and may be too large by a factor of two. It does, however, indicate the large amplification of the particle signal produced by the Cerenkov effect. If other mechanisms of light production by cosmic radiation are considered, as is seen in the data of Table 2.1, Cerenkov radiation is the only one which possesses both an adequate light yield and observed directionality. Light from the ionization and recombination process would be attenuated by the inverse square law and therefore a weak competitor to Cerenkov radiation, except perhaps at large core distances in giant showers of $10^{19} - 10^{20}$ eV. The Fly's Eye experiment in Utah, U.S.A., described by Bergeson (1975) will employ this light to study the highest energy cosmic rays. The Cerenkov radiation produced from an EAS will not be significantly affected by dispersion, diffraction or refraction, see Jelley (1967). The continuum radiation from the night sky, 6.4×10^{7} photons $cm^{-2} s^{-1} sr^{-1}$, peaks towards the red end of the spectrum (showing a six-fold increase in flux from 350 nm to 650 nm). This will not severely interfere with the detection of Cerenkov light because, from Equation 2.1, there is an inverse square relationship between flux and wavelength for Cerenkov light and therefore the Cerenkov light spectrum will peak towards the blue. Photomultipliers employed in Cerenkov light detectors should therefore be most efficient in the green/blue part of the spectrum.

A detailed description of the effect of Rayleigh scattering, ozone absorption and aerosol attenuation is given by Elterman (1968). Their effect is important and such they they must be included in any computer simulation of the radiation.

According to the data summarized in Table 2.1, the angle of emission of Cerenkov light is approximately 1.3^{o}; the confirmation of this by Jelley suggested that the light will retain information about the direction of the emitting electrons. If the light maintains its direction

TABLE 2.1

PROCESS	ASSUMPTIONS	ANGULAR DISTRIBUTION	ENERGY LOSS dW/dl (eVcm^{-1})
Cerenkov	$E_e \sim 100$ MeV	$\sim 1.3^0$	~ 0.8
Ionization & Recombination	Lifetime of the states $< 5 \times 10^{-8}$s	Isotropic	$< 8 \times 10^{-3}$
Synchrotron	$E_e = 3 \times 10^{10}$eV	In vacuo (mc^2/E)	1.3×10^{-7}
	$E_e \sim 10^8$ eV	In air 1.3^0	$\sim e^{-50}$ of this
Bremsstrahlung	$Z = 7$, nitrogen $E_e \sim 100$ MeV	Same as for synchrotron radiation	$< 4 \times 10^{-5}$

through the atmosphere then the lateral spread of light at the observation level can be related to the lateral spread of electrons higher in the atmosphere.

2.3 Previous measurements of Cerenkov Light from EAS

In this section the results of those previous measurements are summarised which relate directly to the work of this thesis, namely measurements in large cosmic ray showers. There have been many measurements in small showers but rather few of large showers using comprehensive systems of Cerenkov detectors in large particle detector arrays.

The first such experiment in large EAS was conducted on Mt. Chacaltaya, Bolivia (altitude 5200 m) by Krieger and Bradt in 1966 and 1967 using nine atmospheric Cerenkov light detectors covering an area of 0.18 Km^2. Inside this was arranged the particle detectors covering an area of 0.07 Km^2. Data from the particle detectors provided the size, core location and the arrival direction of each EAS. They assumed that the incident Cerenkov light was a plane wave parallel to the arrival direction of the EAS. Chantler et al., (1979) have more recently shown that this is not to be the case and the non planarity is of physical meaning. Krieger and Bradt observed showers at core distances less than 350 m and derived an expression for the lateral distribution of Cerenkov light, in the range 75 to 200 m from the core as

$$Q \propto \int_{75m}^{200m} KN^{0.7} exp(-\alpha r + \beta r^2) dr$$

where N is the number of electrons reaching the observation level and for this expression

$$10^{6.5} \leqslant N \leqslant 10^{7.5}$$
$$\alpha = 3.3 \times 10^{-2} m^{-1}$$
$$\beta = 7.1 \times 10^{-5} m^{-2}$$

and K is a parameter which characterises the EAS.

An array of 3 Km^2 area was established at Yakutsk, Siberia, USSR (altitude 100m) in 1971 to record the Cerenkov light and particles from high energy showers. As in the Mt. Chacaltaya experiment, the size, core location and arrival direction of the EAS was determined by using data from the particle detectors.

In 1973 Dyakonov presented the results from Yakutsk which differed from those from Mt. Chacaltaya; the discrepancy was partially accounted for by Krieger and Bradt's 50% uncertainty in calibrating their Cerenkov light photomultipliers. Dyakonov showed that the Cerenkov light flux over the core distance range 300 to 500 m at sea level was independent of cascade model and depended almost linearly on the primary energy of the initiating particle. He gave an expression for the Cerenkov light flux at a core distance R, over the range 0 to 2000 metres as

$$Q(E_o,R) = \int_0^{1020 g cm^{-2}} q(R,X) \cdot N_e(E_o,X) \cdot k(X) dx \quad quanta \ m^{-2}$$

where $q(R,X)$ is the number of photons per cascade electron at core distance R coming from an atmospheric depth X, $N_e(E_o,X)$ is the number of electrons present in the EAS at the atmospheric depth X, and $K(X)$ is the average atmospheric transmission coefficient for the Cerenkov light.

2.4 The Haverah Park Cerenkov Light Experiment

Boley (1964) first suggested that information on the shape of the longitudinal electron cascade was contained in the Cerenkov light pulse. Analysis of these pulses should show how the electron cascade develops, this being the most direct measure of the initiation and growth of the shower and thus the nature of the primary particle.

The Durham group being new in this field, designed an experiment involving techniques specifically aimed at estimating the longitudinal cascade of showers. Their array comprised of eight Cerenkov light

detectors, seven of which were colocated with particle detectors, and covered an area of 0.3 Km^2, see Figure 2.2

Three main measurements were made with this equipment:-

(a) lateral distribution of the light pulse in the range ~ 100 - 500 m,

(b) pulse shapes of the signal recorded at $\gtrsim 200m$ core distance, and

(c) synchronized time of arrival of all detector signals.

(a) <u>The lateral distribution function</u>

An estimate of the total photon flux in an EAS is obtained by taking the integral, over all core distances, of the flux at participating detectors. Figure 2.3. shows the computed lateral distribution of Cerenkov light in showers of energy 10^{16} - 10^{18} eV initiated by various primaries at (a) sea level (1016 g cm^{-2}), and (b) a depth of 835 g cm^{-2}. Figure 2.4. shows the lateral distribution of Cerenkov light for proton initiated showers at various energies. Figure 2.5 shows the lateral distribution of Cerenkov light for various individual showers at 10^{17}eV showing the extreme fluctuation in depth of maxiumum. From these two figures it can be seen that the photon density at a core distance of about 200 metres is virtually independent of cascade development and only relates to primary energy (for energies E $\approx 10^{17}$eV). At Haverah Park the flux density at a core distance of 200 metres, $\emptyset(200)$, has been found to be an adequate primary energy estimator after comparison with the established energy estimator ρ (500 m).

(b) <u>Pulse shapes</u>

If an electron cascade is considered in terms of eight sub-showers (Figure 2.6), then the Cerenkov light emitted by each of these will allow the origin of the pulse shape to be established. Figure 2.7 shows the resulting lateral distributions for each sub-shower. Figure
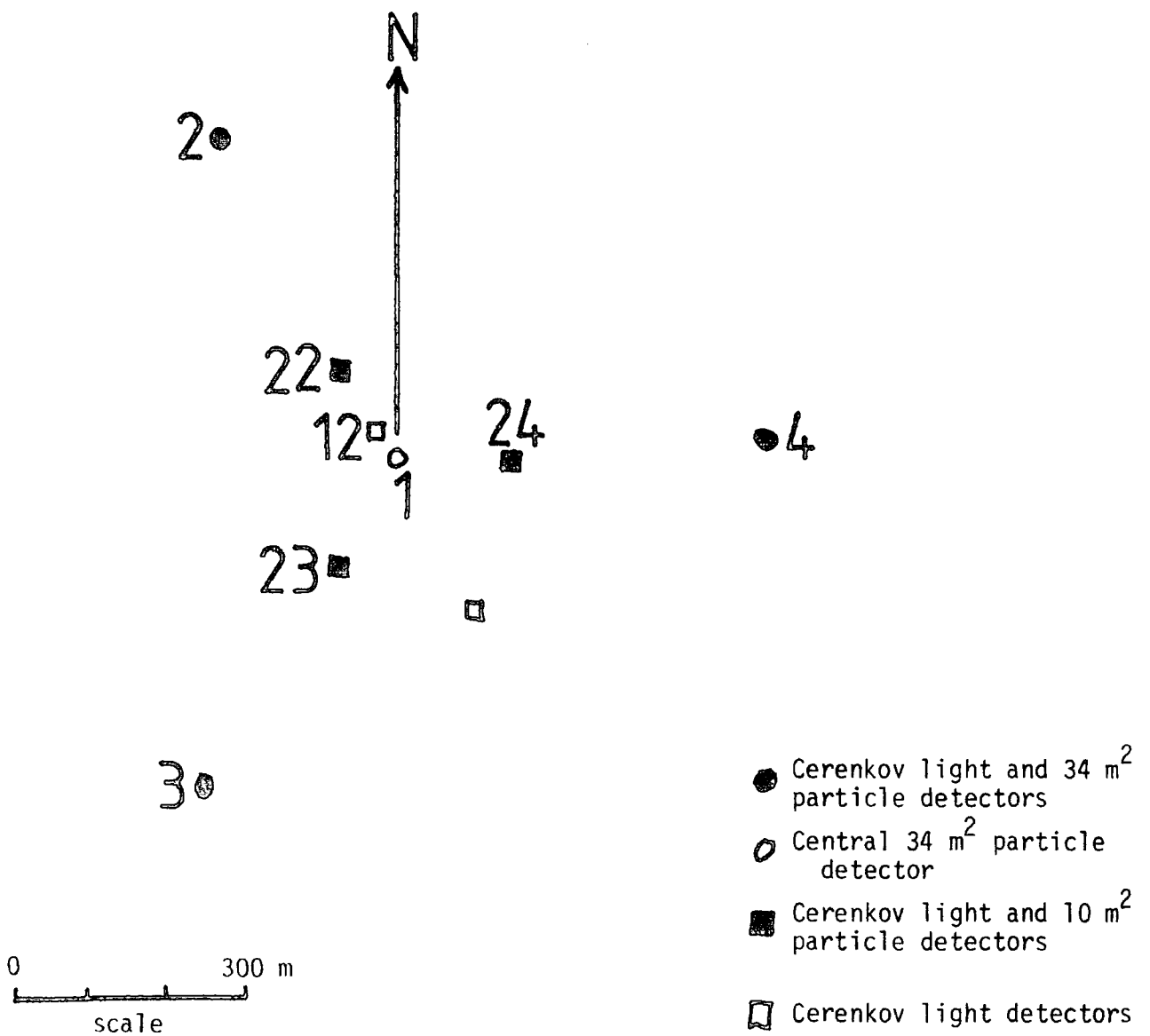
N

2●

22■

12□

○
1

24
■

●4

23■

□

3◐

● Cerenkov light and 34 m^2
particle detectors

○ Central 34 m^2 particle
detector

■ Cerenkov light and 10 m^2
particle detectors

□ Cerenkov light detectors

0   300 m

scale

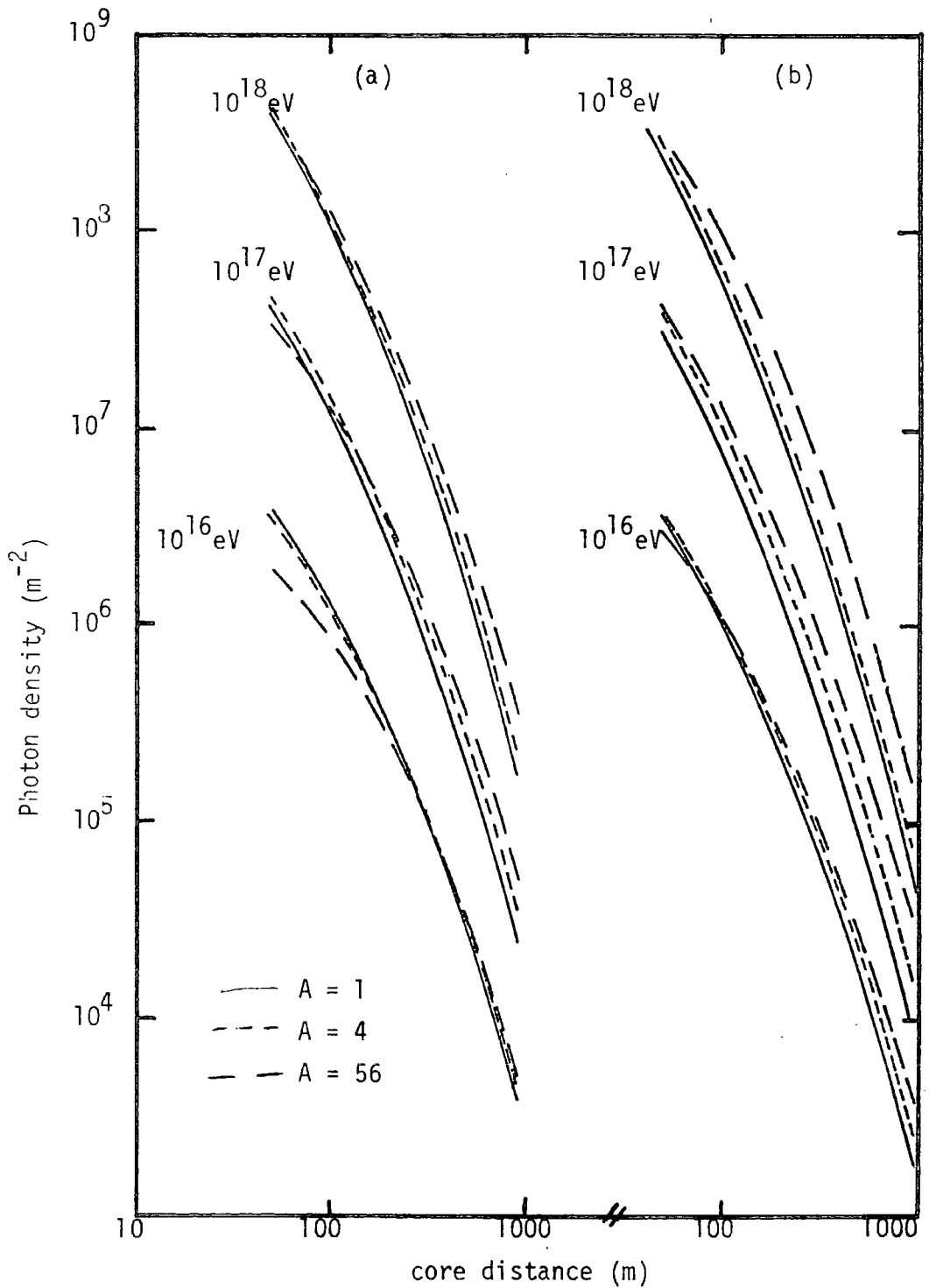Figure 2.2   The Haverah Park Extensive Air Shower Array

Figure 2.3   The lateral distribution of Cerenkov radiation at
(a) sea-level (1016 g cm^{-2}) and (b) a depth of 835 g cm^{-3}
in showers of energy (10^{16} - 10^{18}) eV initiated by
various primaries.

Figure 2.4 Lateral distribution of Cerenkov light for proton initiated showers at various energies.
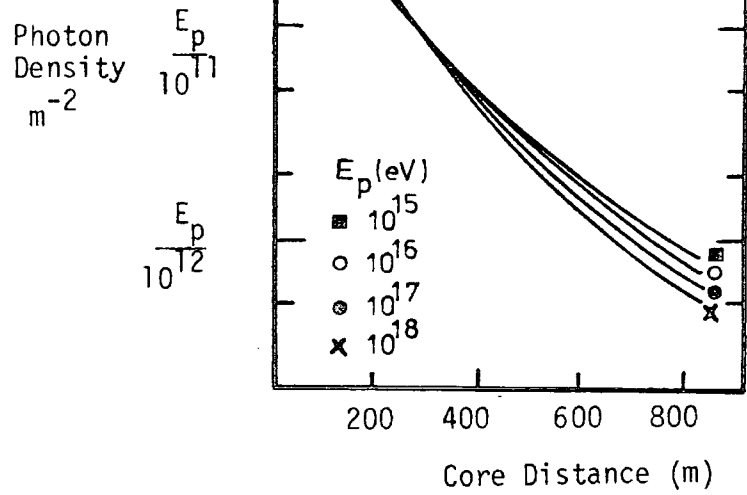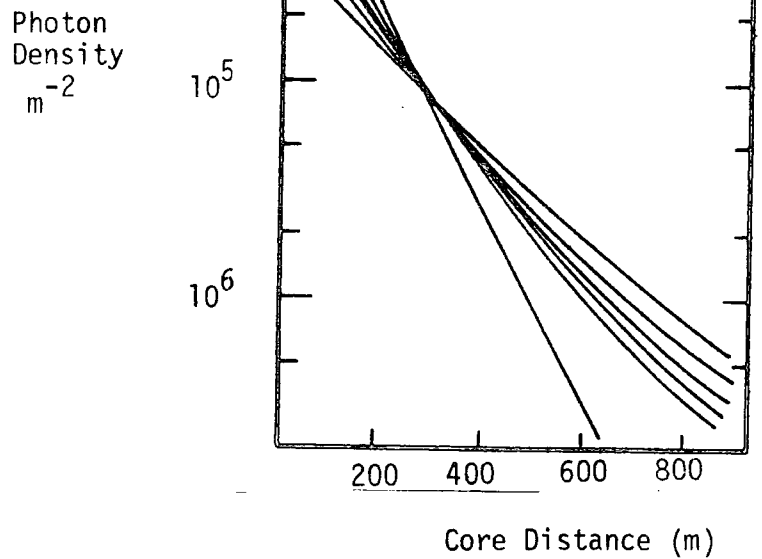
Smith and Turver (1973)

Photon Density m^{-2}

$\dfrac{E_p}{10^{11}}$

$\dfrac{E_p}{10^{12}}$

E_p(eV)
- ■ 10^{15}
- ○ 10^{16}
- ⊕ 10^{17}
- ✕ 10^{18}

200   400   600   800

Core Distance (m)

Figure 2.5 Lateral Distribution of Cerenkov light for various showers at 10^{17}eV

Smith and Turver (1973)

Photon Density m^{-2}

10^5

10^6

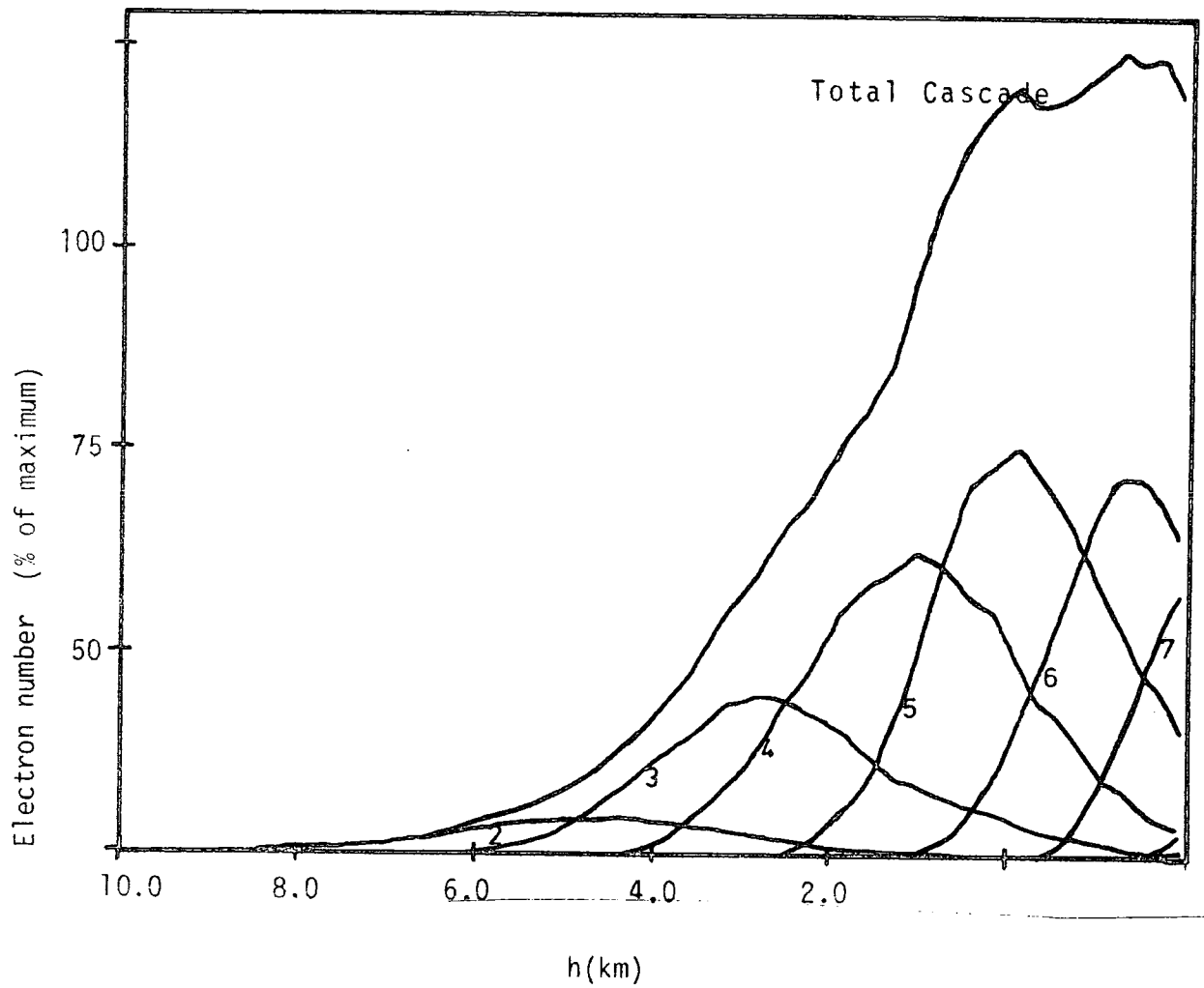200   400   600   800

Core Distance (m)

Figure 2.6 The electron cascade development in a 10^{17} eV proton-initiated shower shown segmented into eight subshowers.
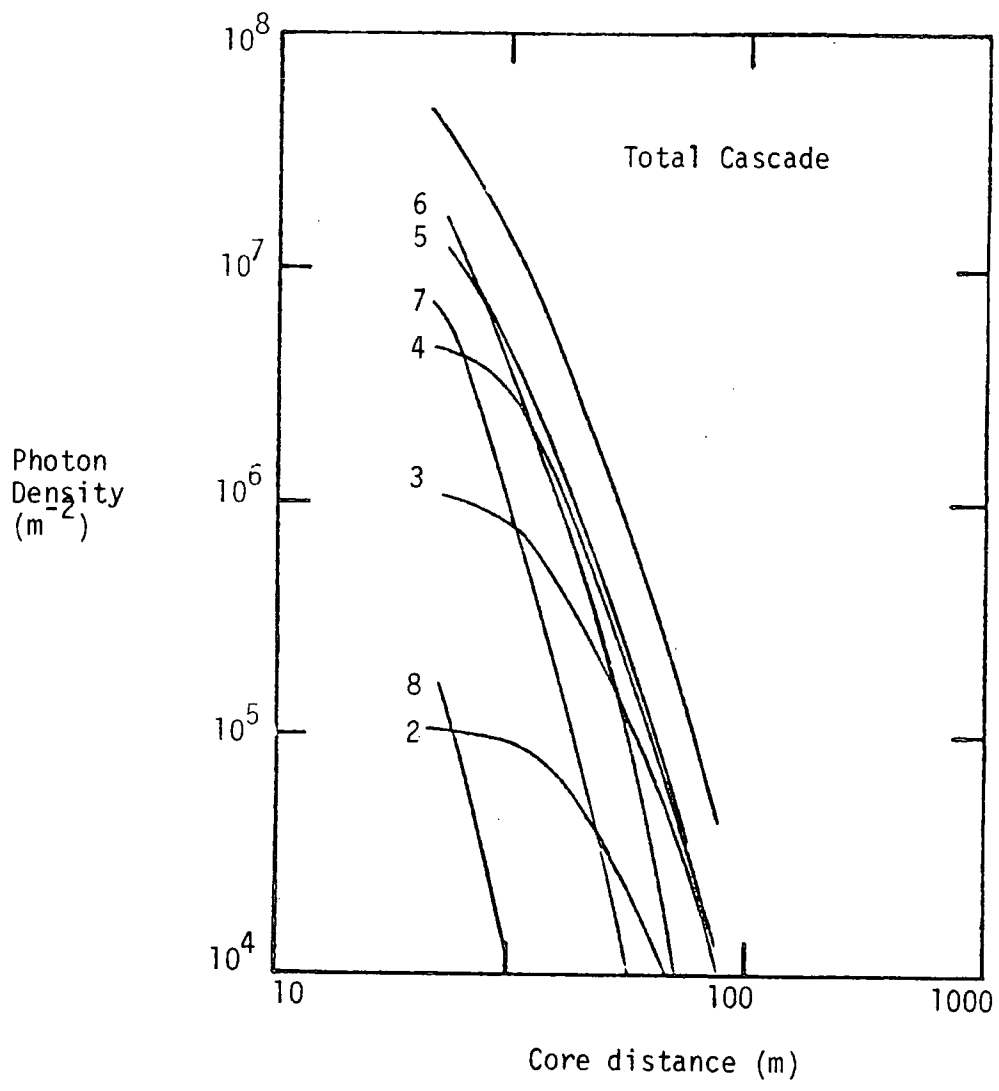
Figure 2.7   The lateral distribution of Cerenkov light in a 10^{17} eV proton initiated shower showing the contributions from the eight subshowers of Figure 2.6

2.8 shows the ground level Cerenkov pulses of light (in terms of the sub-showers shown in Figure 2.6) at various times in pulses at different core distances. For core distances greater than 150 metres it can be seen that the Cerenkov pulse maps directly the electron cascade. The rise time of the pulse gives information about the start of the cascade, the FWHM the situation of maximum development and the fall time, the decay of the shower.

(c) Synchronized time of arrival

The time response of the Cerenkov light detectors were accurately synchronized in order to measure the shape of the Cerenkov light front and derive the arrival direction.

The height of origin of Cerenkov light, detected at small core distances, say 50 metres, has been shown by Bradley and Porter (1960), Boley (1961) and Malos (1962) to be between two and three kilometres. By constructing spherical fronts through various levels of the Cerenkov light pulse shown in Figure 2.8 it is found that for light recorded at core distances of 150 to 600 metres the origin is much higher in the atmosphere, see Figure 2.9. Spherical fronts for the light level were chosen because of their close representation of measured times and the small deviation from calculated points from such shapes. The light fronts thus produced confirm the suggestion that the light in the Cerenkov pulse maps the longitudinal cascade of electrons.

2.5 Separation of Particle and Light Fronts

It has already been shown that Cerenkov light is produced in the atmosphere over a range covering several kilometres. Guzhavin et al., (1975) showed that the light originating highest in the atmosphere reached ground level first, for core distances less than 50 metres.

Considering a photon emitted from the axis of a vertical shower

Core Distance = 50.0m

Total

Core Distance = 200.0m

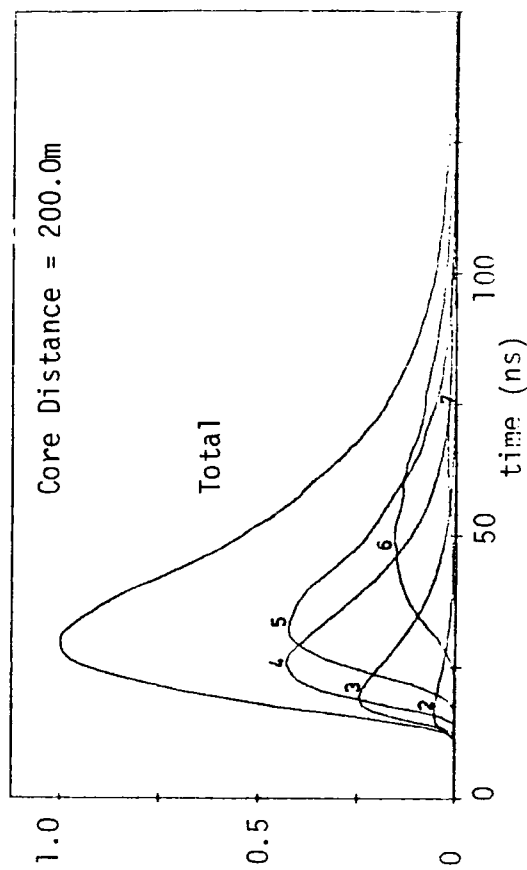Total

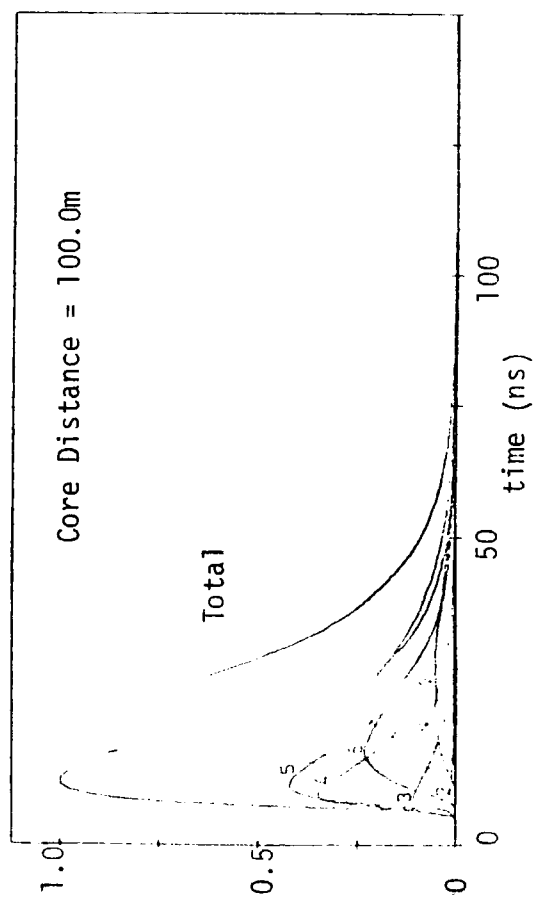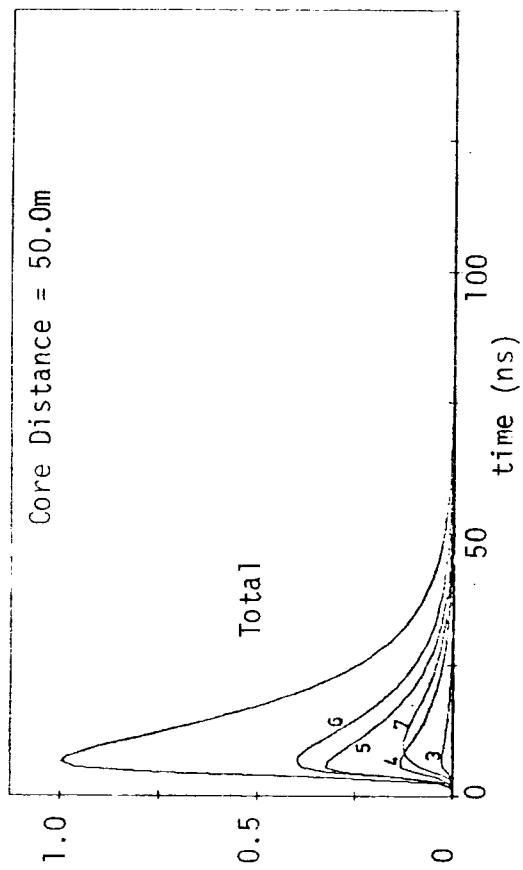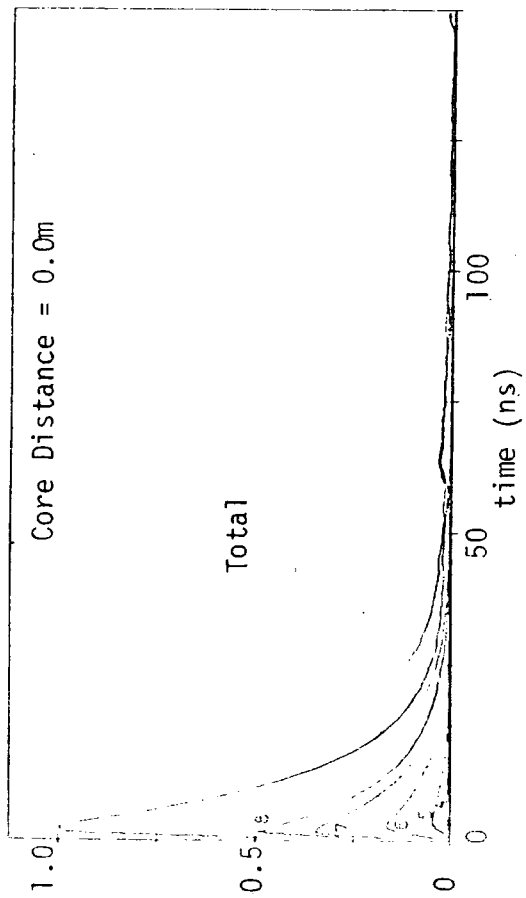Core Distance = 0.0m

Total

Core Distance = 100.0m

Total

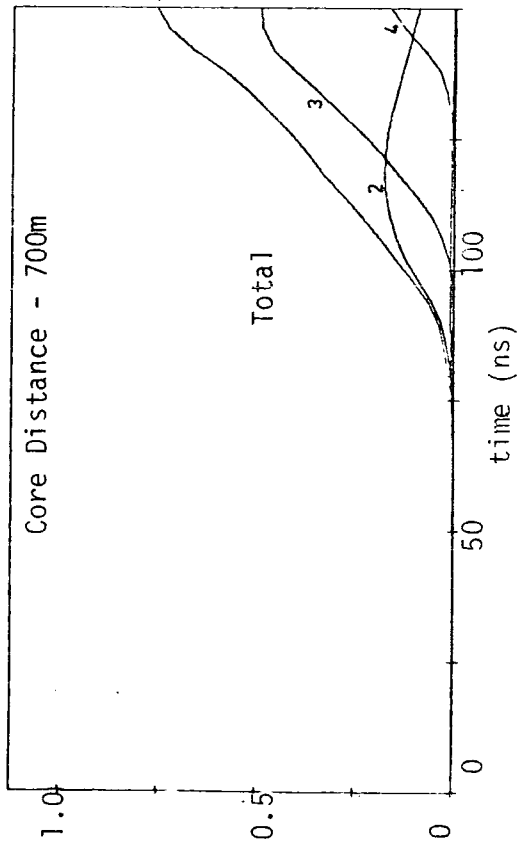Figure 2.8 Ground level Cerenkov pulses of light in terms of the subshowers shown in Figure 2.5
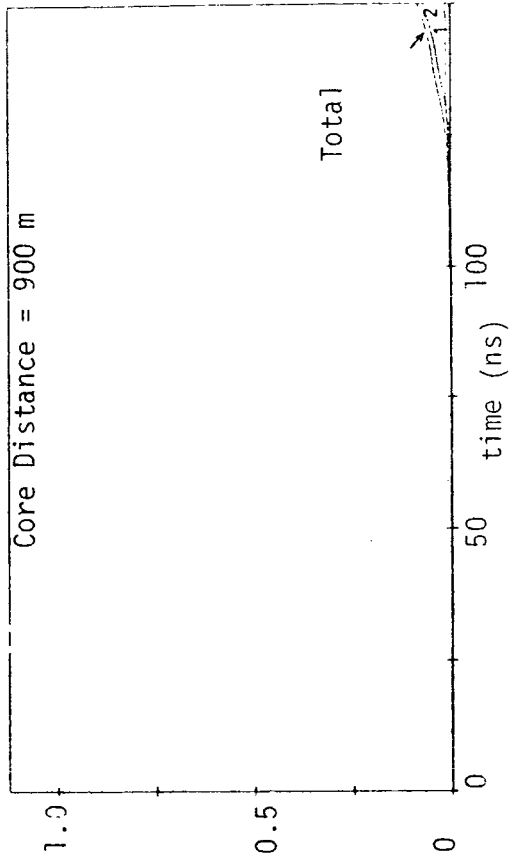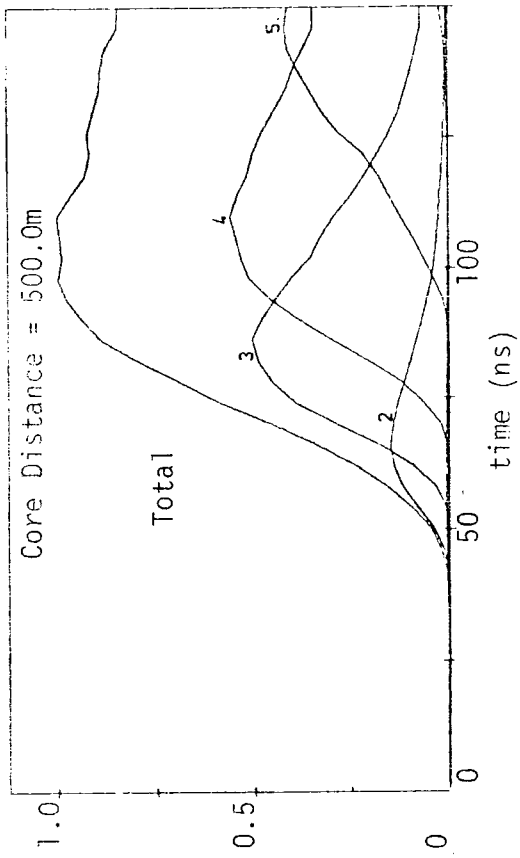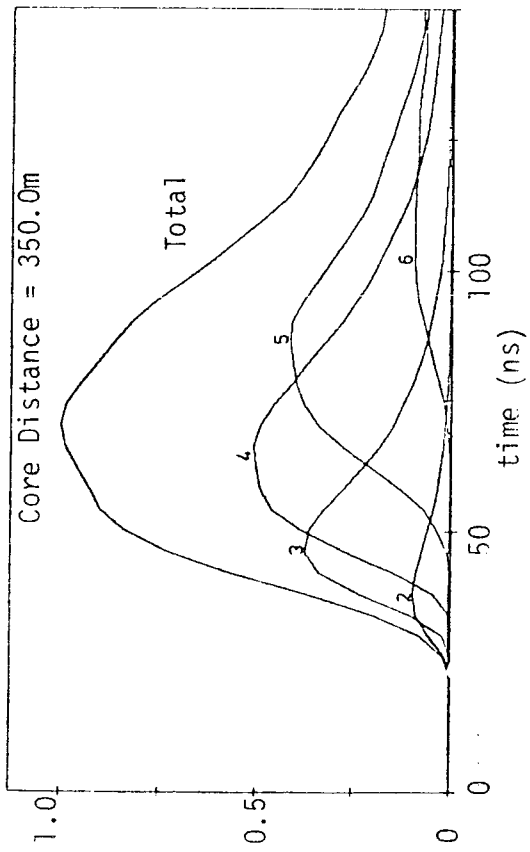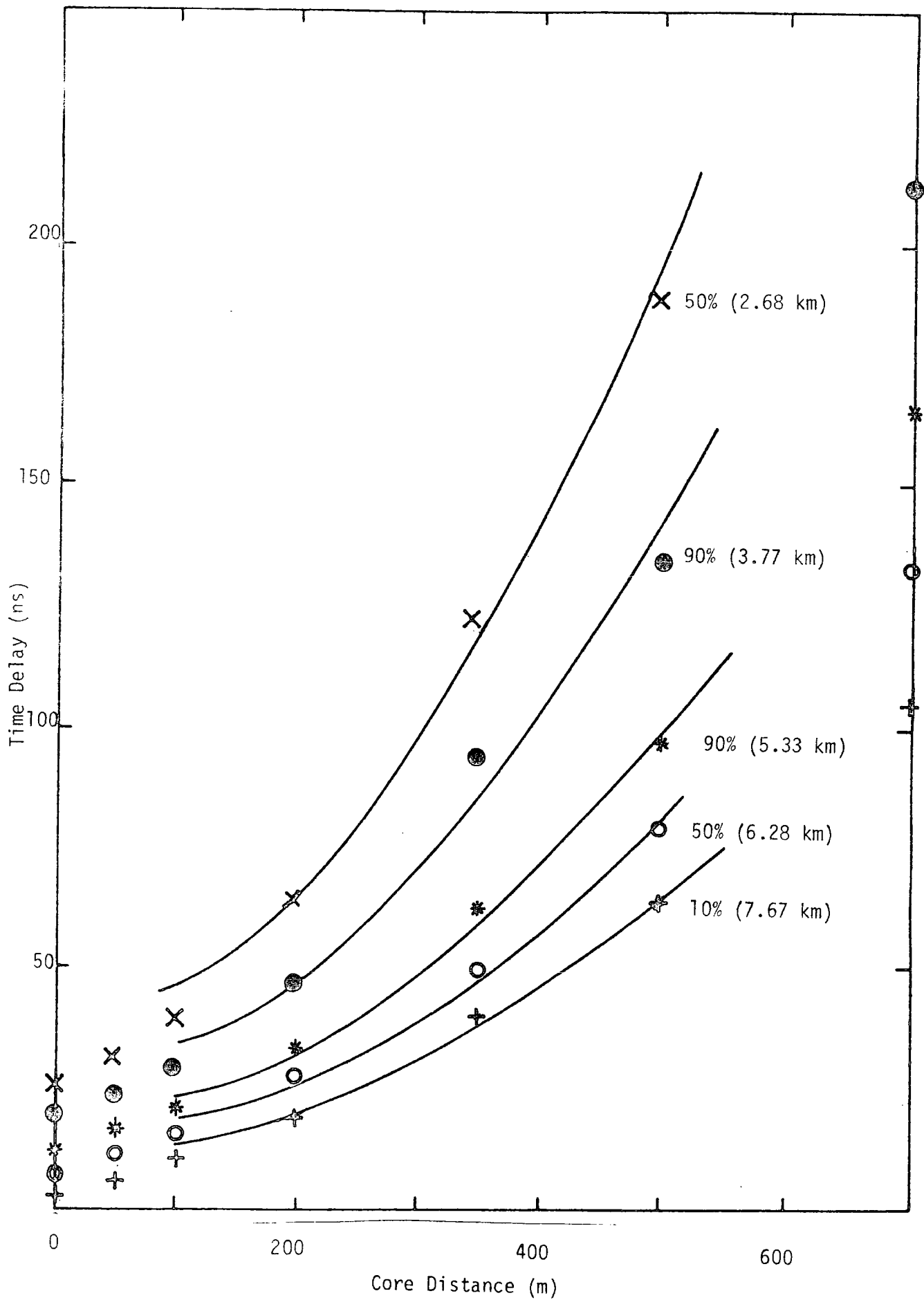
Figure 2.8   (continued)

Figure 2.9   Spherical fronts through various levels in the Cerenkov light
pulse shown in Figure 2.7

at an altitude h and at a time t = 0 and it being detected at ground level at a core distance of r, then the time of detection is given by:

$$t(h,r) = \frac{\sqrt{h^2+r^2}}{c} + \frac{H}{c}(n_0-1)\left[1 - exp\left(-\frac{\sqrt{h^2+r^2}}{H}\right)\right]$$

where H is the atmospheric scale height (7.2 km)

n_0 is the refractive index of air at sea level.

The first term represents path length differences and the second refers to refractive index delays. Figure 2.10 shows the time delay between photons originating at altitude h and those originating at an altitude of one kilometre assuming that the particles causing the emission travel between height h and one kilometre at velocity c.

Cerenkov light will travel at a velocity c/n, where n is the refractive index of air. The particles must therefore be travelling at a velocity in excess of this and so they should reach the observational level before the light. This may be the case at core distances less than 50 metres where the light is local in origin but at greater core distances this is not so. The Cerenkov light and particles have a

closer   common origin, so those originating higher in the atmosphere have about 30 radiation lengths to traverse before reaching the observation level. The rms scatter angle for shower electrons is of the order of 12^0 thus showing that they have undergone perpendicular as well as transverse motion, i.e. they have suffered path length delays whereas the Cerenkov light has not. Therefore at core distances greater than about 50 metres we can expect the light to precede the particles by an amount related to the core distance and the height at which both were coincident, the latter depending upon the primary energy of the initiating particle and its zenith angle of arrival, together with the detail of individual cascade developments.
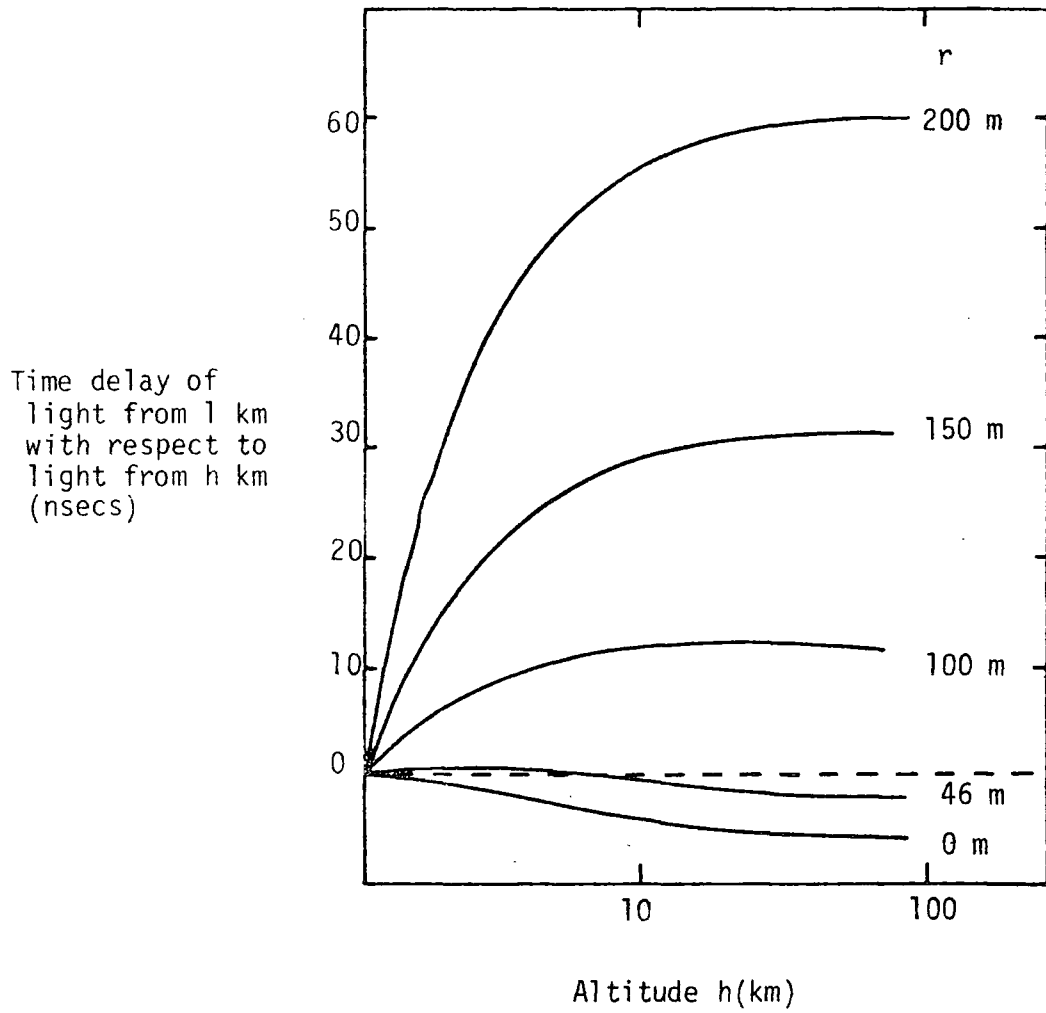
Figure 2.10   The time delay of light originating at an altitude of
1 km with respect to that originating at h km as a
function of h.

2.5.1 Haverah Park Measurements

As mentioned earlier, three quantities were recorded, the lateral distribution, the pulse shape and the synchronization between pulses relative from one detector to another. What was needed to complete the investigation was a measurement that related the absolute time of the Cerenkov light to some other reference. This measurement became the absolute time of the Cerenkov light relative to the associated particle component of the shower, hence the idea of the time delay between light and particle fronts. Using the array as shown in figure 2.1, Shearer (1978) undertook an exploratory experiment and obtained values of the time delay at various core distances. He used the existing large area water detectors which were not specifically designed for fast timing measurements and also fast plastic scintillator detectors which had the right time response but were small in area. A detailed description of the array can be found in Wellby (1978).

The principle findings of the experiment were that the time delay between the light and the particles shower $\sim 10^{17}$ eV was well behaved and at core distances of 150 metres or so, it was shown that Cerenkov light preceded the particles by about 30 ns. Table 2.2 shows a comparison between the experimental results and those from simulations. Chantler et al., (1979) using similar equipment at the Dugway Array obtained a time delay of about 40 ns at 150 metres, this delay increasing by about 25 ns for each 100 metres increase in core distance, see Figure 2.11.

In the past only the region near the shower axis had been considered by e.g. Malos (1955). The time delays measured in the recent experiments at large core distances (r > 75 metres) behaved quite differently from what had been previously measured or considered to be the correct sequence for the arrival of the particles and light. The further

TABLE 2.2

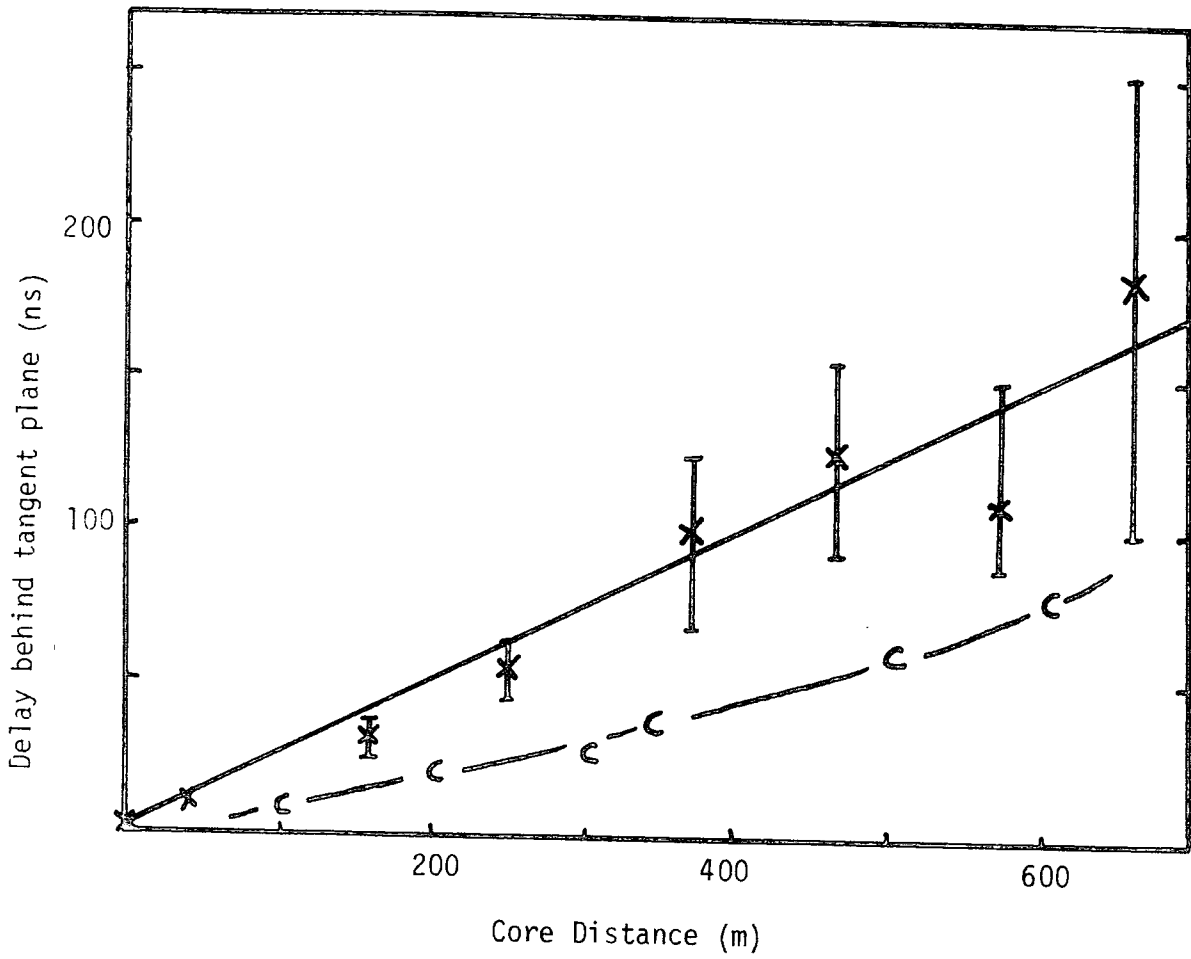| A	nsec/100m @ 10^{17} eV	nsec/decade in energy $10^{16} - 10^{17}$ eV	nsec/decade in energy $10^{17}-10^{18}$ eV	nsec/100 gm (from zenith angle)
1	28	50	20	5
56	25	50	20	-
observed	23	(27	27)	5

Figure 2.11   The time delay behind the tangent plane as a function
of core distance for particles (x) and Cerenkov light
(c) at Haverah Park.

development of our understanding of this time difference and its application as a useful means of cascade development are the prime aims of the work discussed in this Thesis.

CHAPTER III

THE DUGWAY CERENKOV LIGHT EXPERIMENT

Introduction

This chapter describes the atmospheric Cerenkov light experiment
located at Dugway, Utah, which was the environment in which the
measurements of the separation of the particle and light fronts were
made. The Cerenkov light and particle detectors are described
together with the method of data recording. Finally a description
of the analysis of the data is given and the present situation is
reviewed.

3.1 The Array

An array of eight Cerenkov light detectors was established in the
Great Salt Lake Desert, Utah, U.S.A. at an elevation of 1451 m at
latitude 40° 12' North, longitude 112° 49' West. The array was
established in 1977 and the layout is shown in Figure 3.1. The plastic
scintillator particle detectors and the Cerenkov detector coded $\emptyset$ had
not been included when intial measurements were made from October to
December 1977. The array was operated on all nights in the new moon
period; data from clear moonless nights were selected for analysis.
Routine operation, including the scintillators and detector $\emptyset$ began
in October 1978 and continued to April 1979. Showers of energy in
excess of about 10^{16} and 10^{17} eV incident within 45° of the zenith
were recorded at rates of ~5 and 0.5 $hour^{-1}$ respectively. Each
Cerenkov light detector was capable of measuring the pulse area, the
shape and the arrival time to an accuracy that was greater than those
available in earlier measurements at Haverah Park (see Hammond et al.,
1978)).

A second season of measurements were made between August 1979 and
March 1980. By November 1979 300+ hours of clear sky observations had
been made accumulating some 7500 shower records. The array dimensions

N

Y

φ

2

0

7

5

1

4

X

6

0 _____ 200m

3

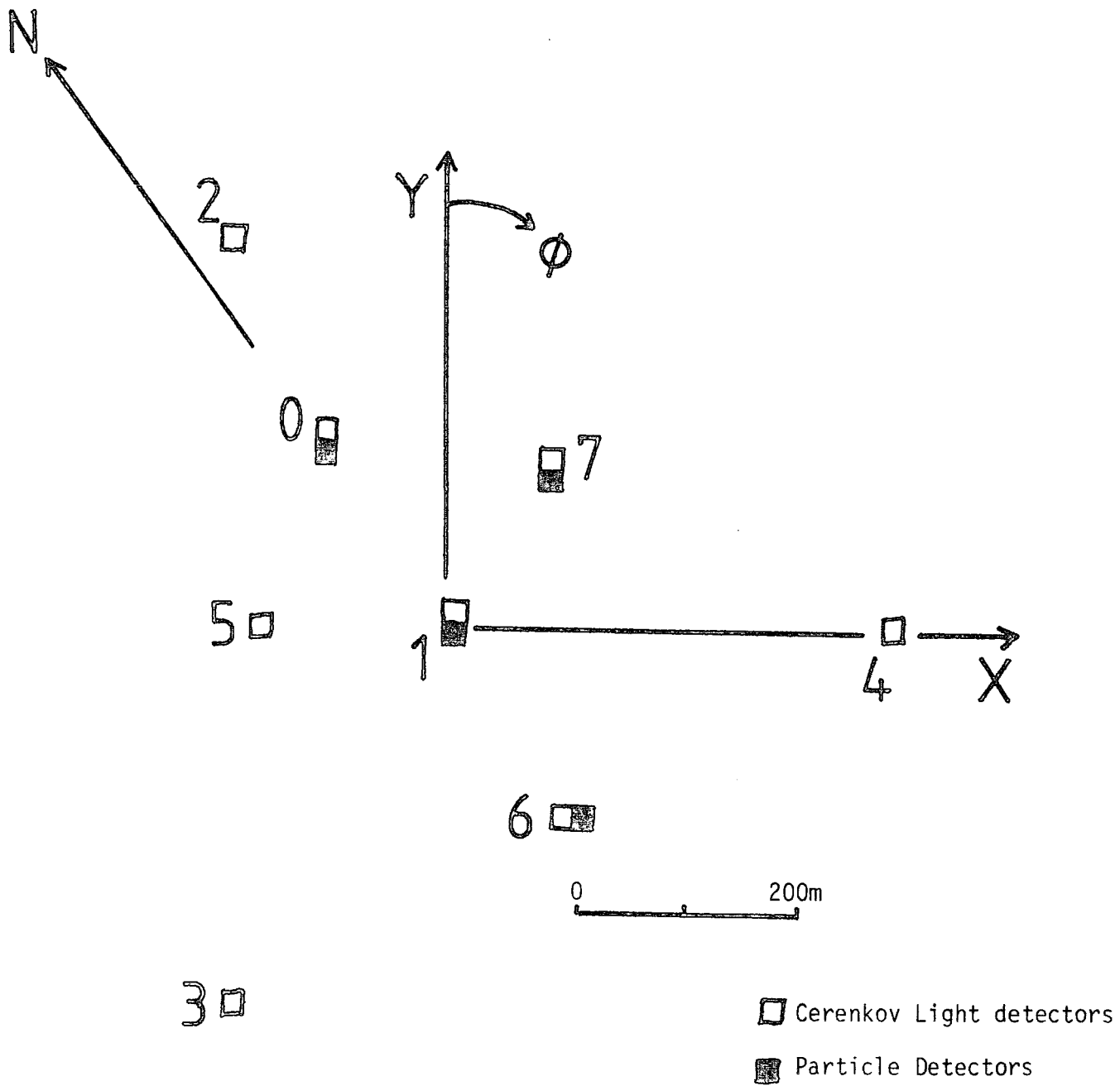☐ Cerenkov Light detectors

▓ Particle Detectors

Figure 3.1   The Dugway Air Cerenkov Array at the start of the
first season of routine operation, October 1978.

Mk 1 Array Configuration

were then reduced to those shown in Figure 3.2, the array sensitive
area being reduced by approximately four. Showers of lower energy
($\sim 10^{16}$eV) were now recorded. During January 1980 the Cerenkov detector
2 was moved twice, see Figure 3.3. These smaller dimensioned arrays
(mark 2,3 and 4) recorded $\sim$7000 showers in 60 hours of clear sky
observation. In February 1980 the array configuration was reduced
again to that shown in Figure 3.4. This final configuration was used
to make observations for 25 hours under clear skies yielding 3000 showers
at energy $\geqslant 10^{15}$ eV.

3.2 The Cerenkov Light Detectors

Cerenkov light detection was achieved using a fast response 12 cm
diameter photomultiplier RCA type 4522 which viewed the night sky through
a 3mm thick perspex window and was located in a temperature controlled
enclosure. The enclosures which were small (60 x 55 x 90 cm) and
contained the associated electronics, were portable, which became
important towards the latter stages of the experiment when all the
detectors except those coded 0 and 1 were relocated twice.

Each detector was supplied with power from a trailer situated near
detector 1. The trailer acted as an operational headquarters and data
collection point. Each detector was linked to the trailer by three
other cables carrying a fast-timing synchronising pulse to the
detectors, the digital data from them and a selection of housekeeping/
monitoring levels from each.

The array was controlled and the data were recorded using a Tektronix
4051 computer. After deciding that the night sky was clear enough or
showed prospects for useful data collection the computer was allowed
to command the detector array "ON". This occurred when the time on
a clock, kept accurate to within one second, corresponded to the time
on an incorporated ephemeris. Upon receipt of the "ON" command, a
motor removed a cover from each photomultiplier thus exposing them to

Figure 3.2.   The Dugway Air Cerenkov Array from 26 November
1979 to 10 January 1980.

Mk 2 Array Configuration

Mk 3 Array configuration (Detector 2 next to detector 0)

Mk 4 Array configuration (Detector 2 50 m from Detector 1)

N

Y ϕ

0 2 (1st move)

7

2
(2nd move)
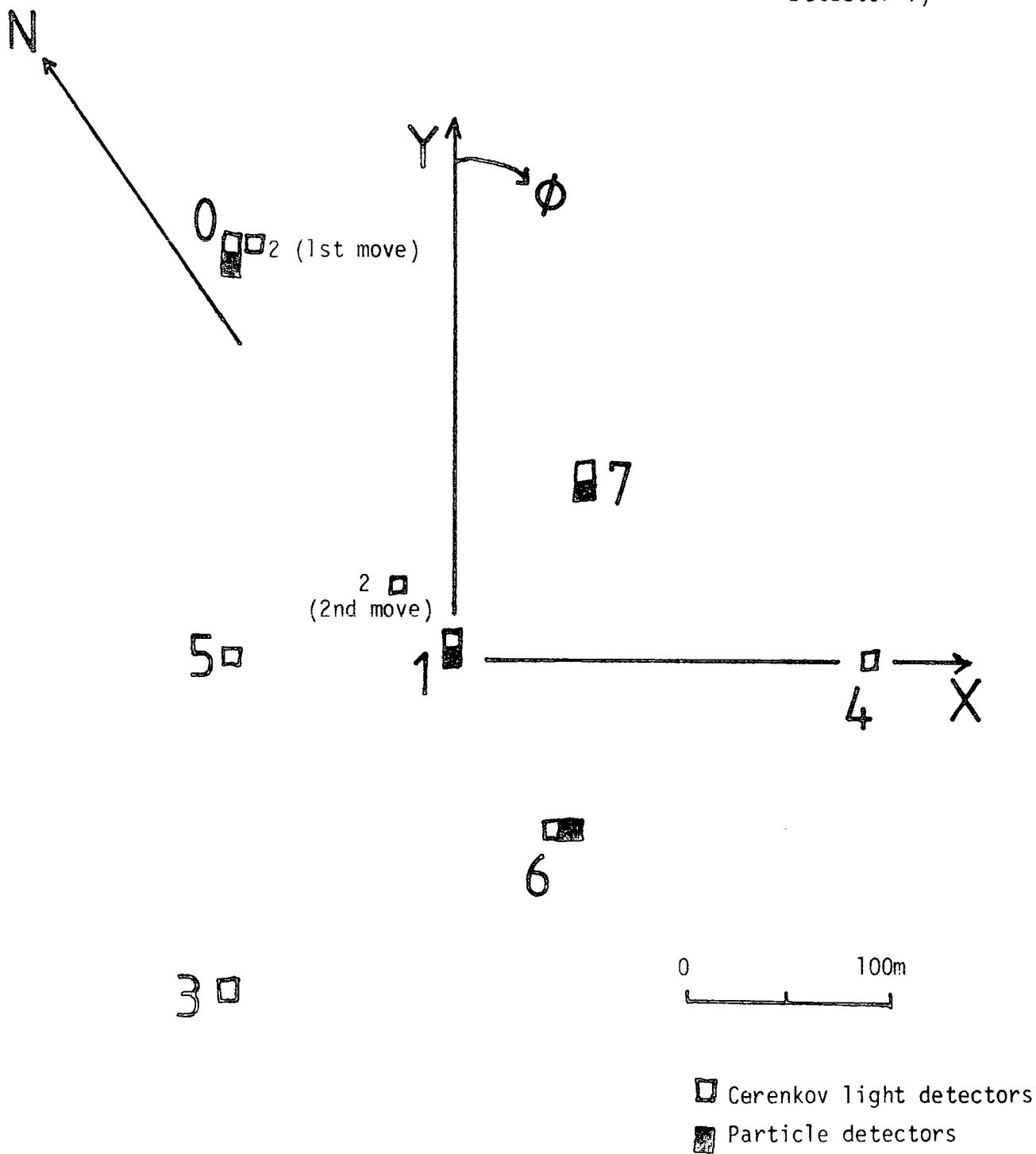
5

1 4 X

6

3

0 _____ 100m

□ Cerenkov light detectors

▣ Particle detectors

Figure 3.3 The Dugway Air Cerenkov Array from 12 January
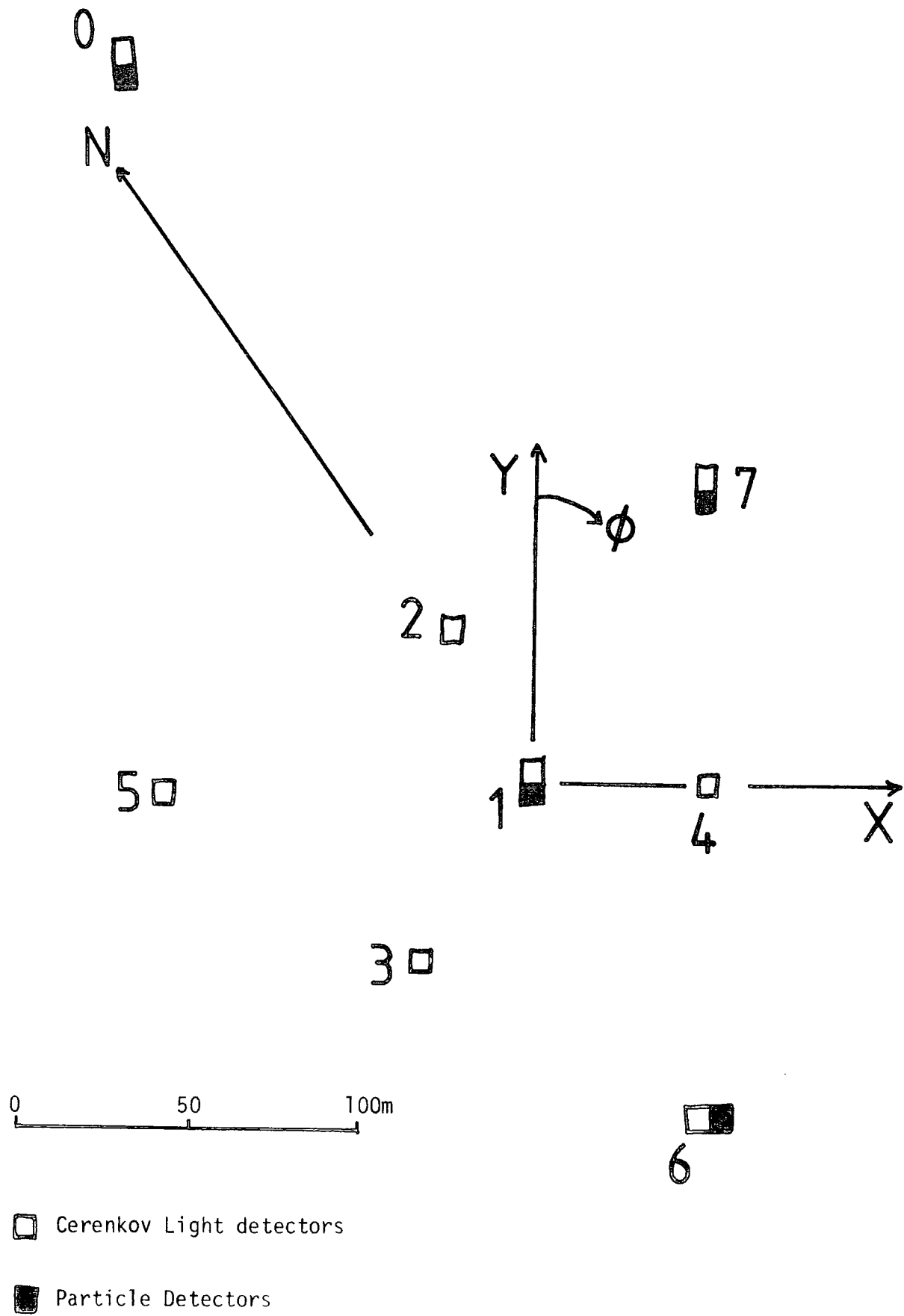1980 to 11 February 1980

Figure 3.4 The Dugway Air Cerenkov Array from 15 February 1980
to 12 March 1980

the clear moonless night sky and applied the high voltage (EHT).

The photomultiplier anode currents were normally 1% of their maximum

rating (500μA). In the event of the current of any tube exceeding 10%

of this maximum the EHT of that tube was turned off automatically. There

was a relatively high photo-cathode illumination by the Cerenkov light,

so each photomultiplier tube was operated at a low overall gain. The

output was taken from the 11th dynode to allow the voltage per stage

to remain high with a consequent fast and non-jittery response. The

signal was then amplified (x 100) by two Le Croy VV100 amplifiers. The

resulting photomultiplier/amplifier gain was 60,000 and the pulse rise

time about 2.5 ns. A schematic diagram of the detector electronics is

shown in Figure 3.5.

Each detector was connected to the computer and central EAS

coincidence electronics by a synchronising cable with a pulse transit

time of 1μs. The Cerenkov pulse was reconstructed by measuring the

charge within 10 ns sequential slices through the PMT signal,

Figure 3.6. Instead of transmitting a photo tube's signal to the

trailer and digitising it there, the signal was digitised at the

detector immediately it passed a discrimination level and then trans-

mitted in digital form to the trailer, thus giving a more accurate pulse

reconstruction. The discrimation level was adjusted at the beginning

of each season by changing the photo tube EHT to give a response rate

for each tube of <10 counts s^{-1} thus giving a small dead time. There-

after the EHT (and gain)remained constant. If an EAS coincidence,

defined as the simultaneous response of any three of detectors 2, 3, 4,

5, 6 and 7 was not generated within 5μs of each detector's response,

the digitisation routine was stopped and the detector reset for the

next pulse.

Figure 3.5 Schematic diagram of the detector electronics
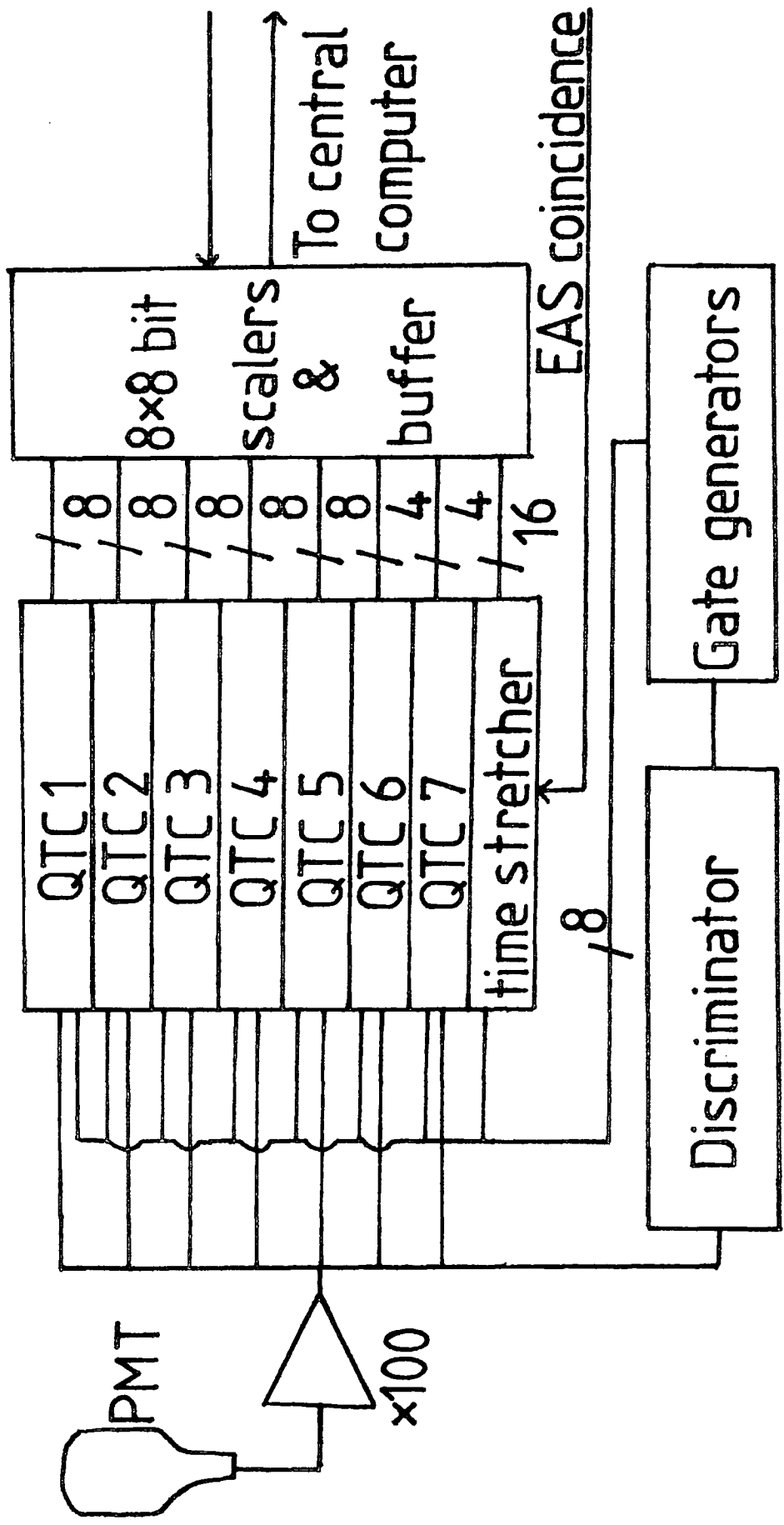
QTC: Charge to time converter. Le Croy QT100B
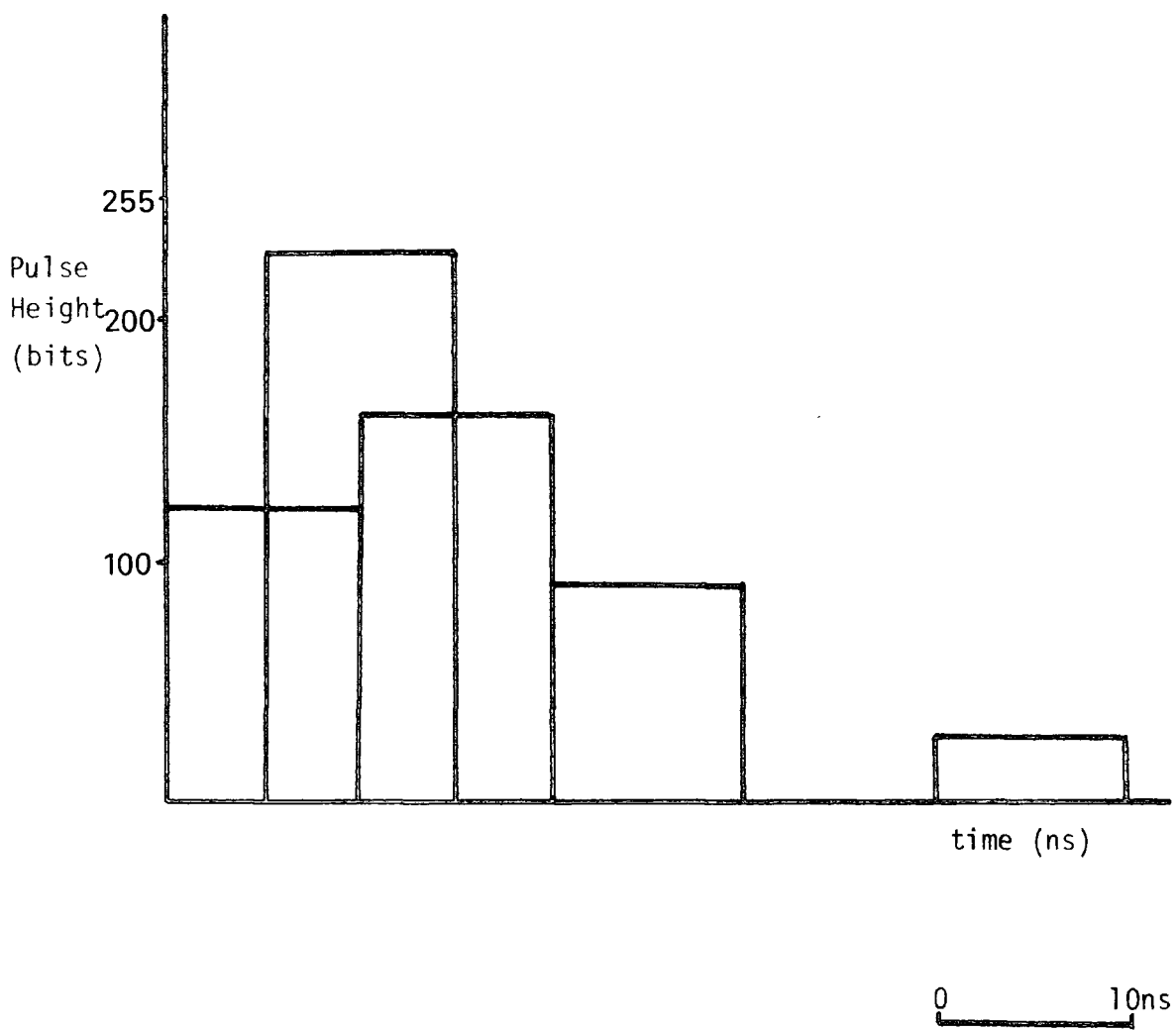
PMT: RCA 4522 in mu metal shield

Figure 3.6 Schematic representation of the sampling through a Cerenkov pulse.

3.3 The particle detectors

Each detector comprised of a $1m^2$ slab of plastic scintillator type NE 102A of thickness 5 cm and viewed from opposite sides by two EMI type 9530 photomultipliers (diameter 12 cm). Each plastic scintillator together with its two photomultipliers was housed in a light-tight, weather-proof and insulated aluminium box and located adjacent to a Cerenkov light detector as shown in Figure 3.1.

3.3.1 Specification of the particle detectors

The specification was to convert each of four particle detector delays between the response of the Cerenkov light detector and the corresponding particle density into voltages between 0 and 5 volts which were maintained for $\geqslant$ 150 ms. Such voltages could be digitised and suitably logged as additional housekeeping data by the computer. (The fixed format of the data logging system precluded the addition of further digital information directly).

The time delay range 0 - 100 ns with simultaneous light and particle signals appearing (as a result of cable delays) as $\sim$ 30 ns was specified; a dynamic range of 50:1 for particle densities was required.

3.3.2 Time delay measurement

Timing measurements were achieved by using a commercial time to amplitude converter (TAC) which was started by the Cerenkov signal derived from the adjacent Cerenkov light detector and stopped by the particle signal derived at a level of approximately 2 particles $/m^2$. The output of the TAC ranged between 0 and 1 volt which corresponded to a time delay of 0 - 100 ns and lasted for 20μs. This signal was offered to a sample and hold circuit which extended the time to 150 ms with less than 5% sag at the end of that time. The voltage was then amplified by a factor of 5 and passed to the trailer where it was

digitised by an eight bit fast digitizer. This gave a readout of 256 bits representing 0 - 100 ns i.e.~0.4ns/bit, accuracy, see Figure 3.7.

3.3.3 The particle density measurement

The particle detector signal was passed to the sample and hold circuit after it was integrated and amplified thus also producing a pseudo-DC level. This voltage was sampled after 5μs if the original signal passed a 200 mV discrimination level (equivalent to ~2 particle/ m^2). If the discrimination level was not reached, a further sampling took place after 15 ms when the integrated signal had decayed away thus effectively resetting the sample and hold circuit. If the circuit received a signal from the trailer (meaning that an air shower detected by its Cerenkov light had occurred) then the sampled signal was amplified and sent to the trailer as a pulse of width 150 ms and height ranging from 0-5 volts. The signal was then digitized in the same manner as that in the previous sub-section. The dynamic range of the particle density measurement was about 100:1.

3.3.4 Calibration of the particle detector system

(a) Timing calibration

An in situ time calibration of the combined Cerenkov light detector and the particle detector was made. This was achieved using a supplementary small-area plastic scintillator slab which was located temporarily above the Cerenkov light detector photomultiplier tube. Operating either at night or in "blacked-out" conditions during the day, the Cerenkov light detector photomultiplier tube responded to the scintillation light produced by cosmic ray particles striking the small temporary scintillator. Particles in the same shower arriving coincidently were detected by the particle detector. It was therefore possible to obtain the digitised time delay for the coincident arrival of signals at the Cerenkov light detector photomultiplier tube and the particle
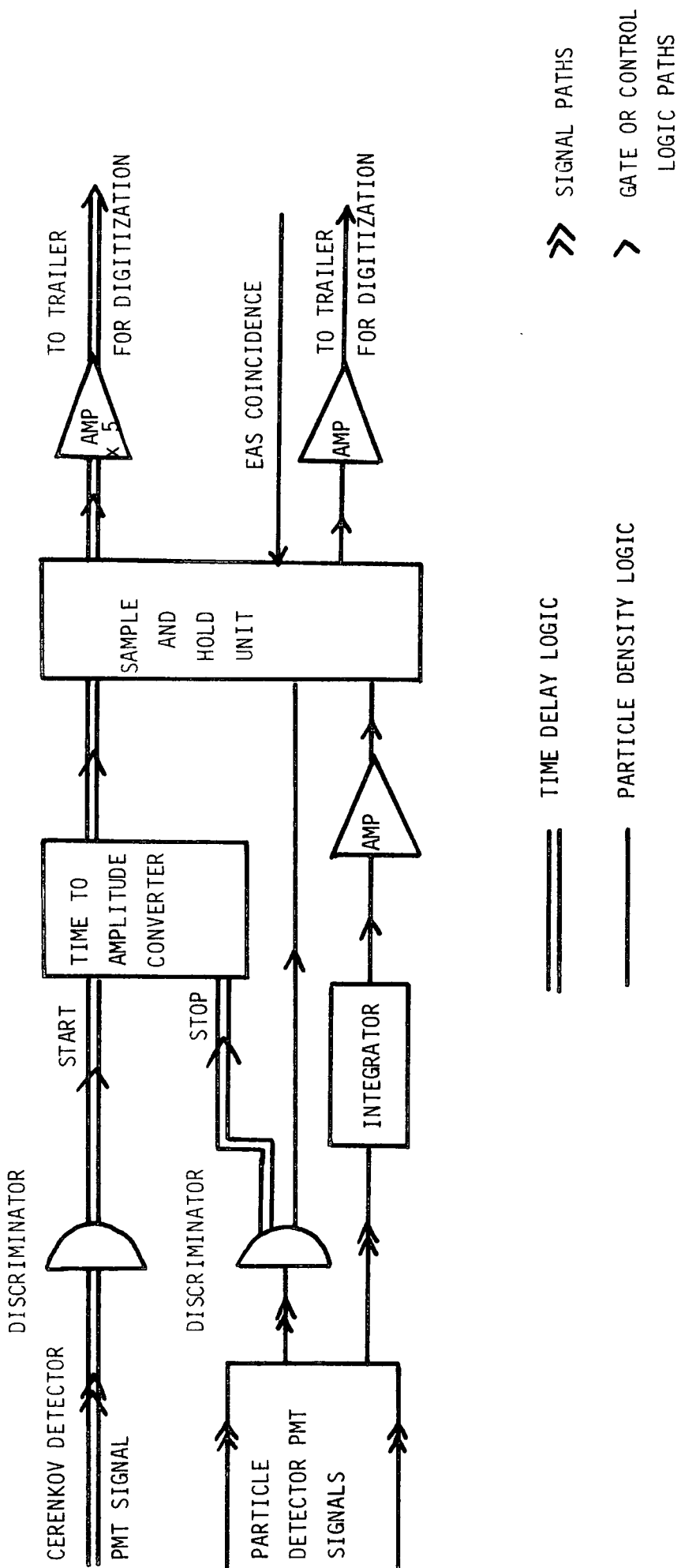
Figure 3.7   Schematic of time delay and particle density electronics

detector. This procedure was repeated with additional lengths of cable inserted into the particle signal's path so that the time delay system was calibrated over most of the 100 ns sensitive region, see Figure 3.8.

(b) Particle density calibration

This calibration was confined to the inter-relation of the relative gains of the detectors, with no attempt being made at an absolute density calibration. The interrelation of the gains was made using the integral cosmic ray spectrum recorded by each detector. This was simultaneously measured at five different discrimination levels and an integral response spectra was obtained for the detectors, see Figure 3.9. The preliminary settings of the gains of detectors $\emptyset$ and 6 had achieved a gain varying from detector 1 by 19.9 and 54.2% respectively.

3.4 Analysis of the data

The timing and density measurements were made in showers in which the Cerenkov light data had been the subject of an initial first look analysis, see Shearer (1980). The data were recorded on DC 300A data cartridges of capacity 1/3 M byte in the form of files. The first record on a file was a housekeeping event which contained the time, the digitized detector temperatures and the data. The second record was a calibration event which contained -

1. The time

2. Various digitized environmental parameters i.e. the atmospheric pressure - the brightness of the night sky (recorded by a separate photomultiplier tube of diameter 2") - the temperature in a sensor box located near Cerenkov detector 1 - the underground temperature (6" depth) - the temperatures at six inches and five feet above ground level.
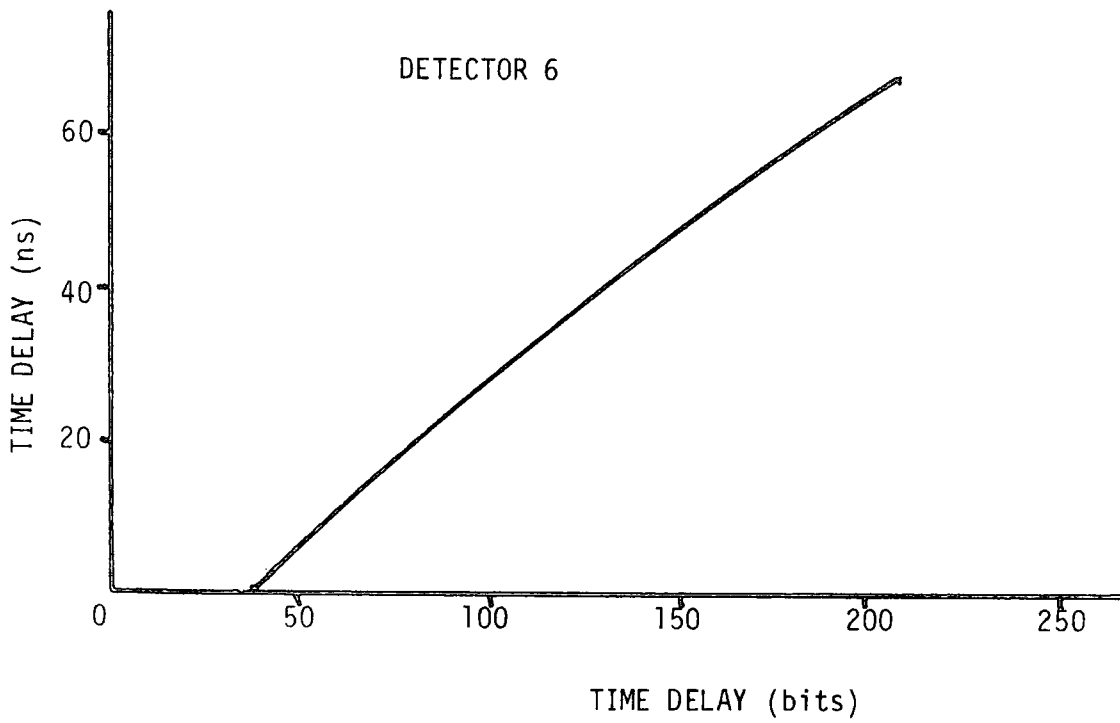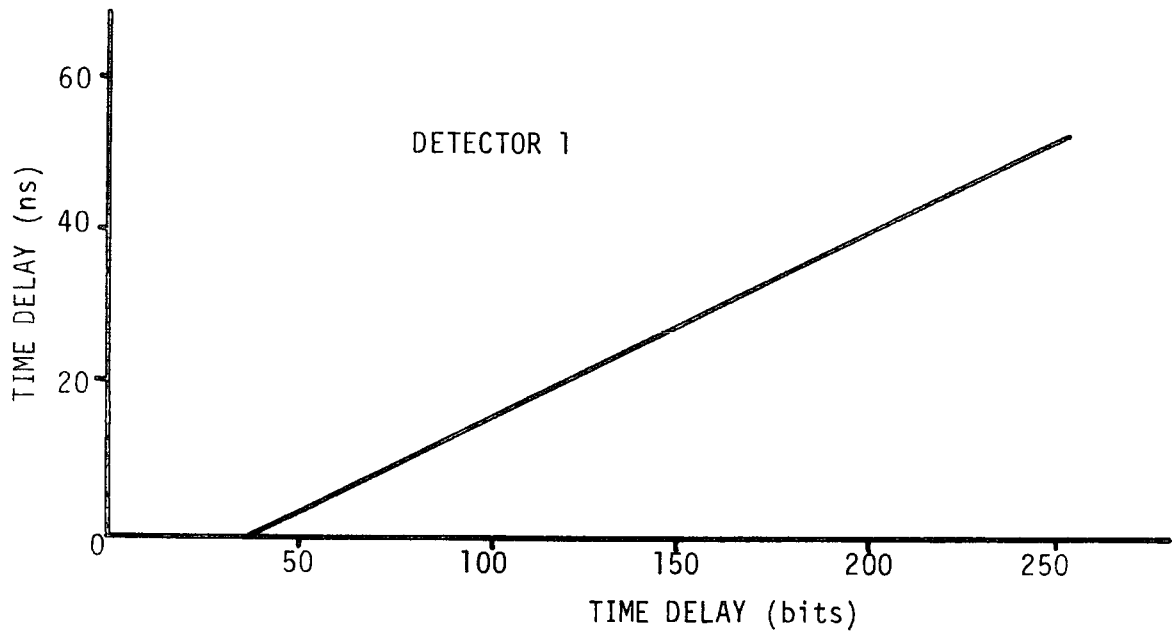
Figure 3.8   The calibration curves for the timing systems of detectors 1 and 6.
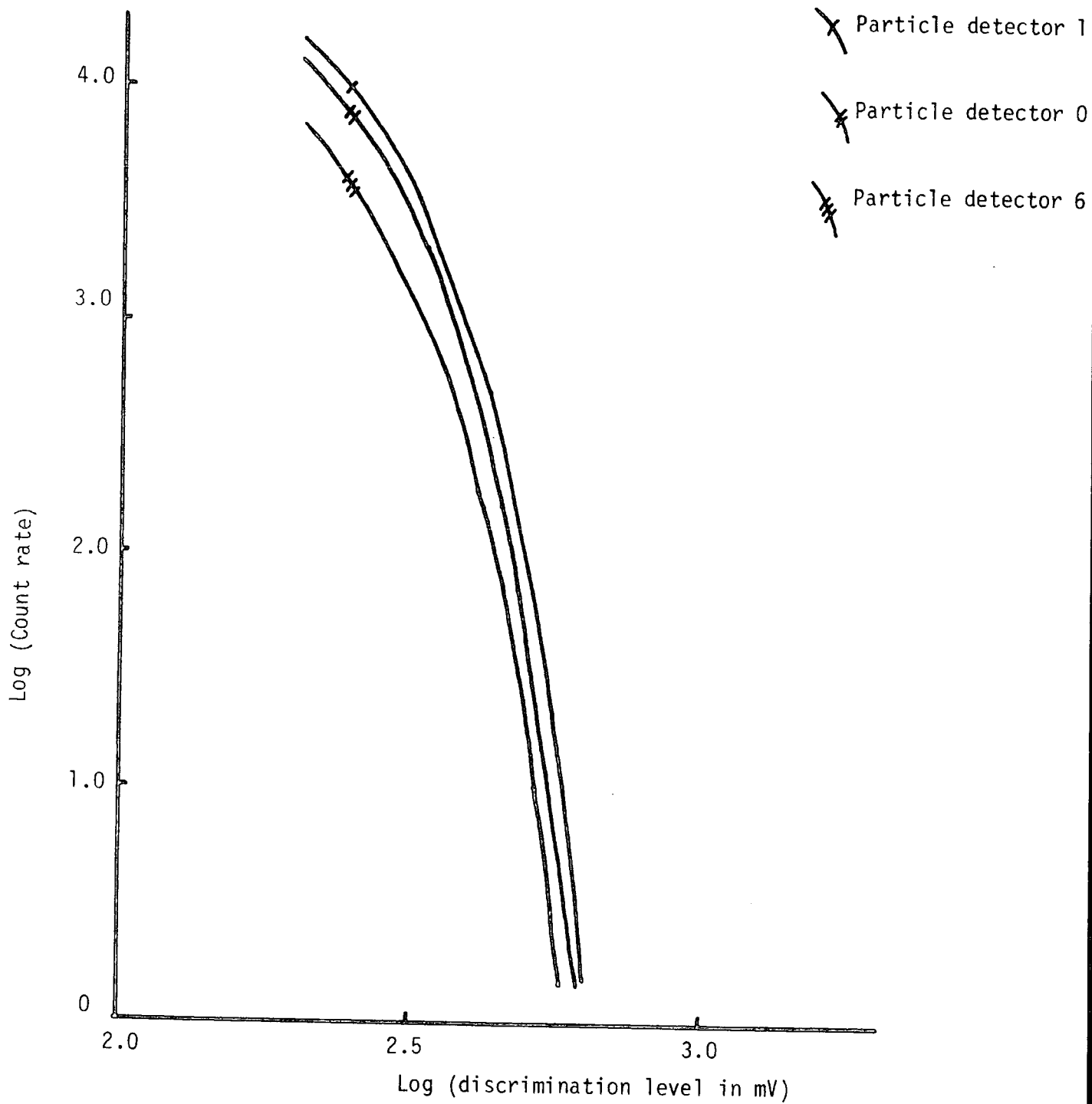
Figure 3.9   The integral cosmic ray spectrum showing relative
gains of the particle detectors

3. The output from each slice measurement with no signal input,
    giving the number of residual bits, i.e. the pedestal of the
    digitization.

The next thirteen records were shower events which contained data in
the same format as a calibration event except that

(1) the output from the particle detectors was now included.

(2) the response from participating detectors representing detected
     pulses.

(3) the participating detectors gave a time of arrival record which
     was used to find the arrival direction of the shower.

The data having been recorded were transferred to computer disk
where it was suitably edited to allow analysis by lengthy computer
programs. The data were split into blocks containing about ten to
fifteen files covering no more than one night's observation. Initial
investigation of the data was carried out using a program (PRESIEVE)
which generated general run information such as:

1. the event rates

2. the frequency of response of 3,4,5 etc. detectors in EAS

3. the average pedestal values for all digitized quantities

4. the individual detector response rates

5. a triggering profile graph, which would show if the trigger
    rate varied due to - e.g. clouds appearing during the
    run-time

6. a pressure profile graph which indicated the atmospheric
    pressure throughout the run period

7. a graph of the night sky brightness throughout the run

8. histograms for each measured quantity of each detector showing
    the frequency of responses recorded when the detector was
    triggered in EAS.

The first look analysis which was applied to every shower record was carried out using a program (SIEVE) which was under constant development throughout the experiment until a final automated version was produced which analysed each event efficiently. This analysis involved a thorough derivation of the arrival direction of each shower based on a MINUIT optimization of the time records. The arrival direction of even the smallest and least suitably measured shower was accurate to a degree or better in zenith and azimuth angle;when compared to the results of earlier experiments, this first look analysis of the arrival direction is very accurate. The core position of the shower and an estimate of the primary energy were also made using a thorough MINUIT-based analysis of the Cerenkov light densities which provided the core distance to every detector, the best fit structure function exponent η for $\emptyset \propto (r + r_0)^\eta$ and a number of possible measures of primary energy. A full study will be required to decide which is the optimum measure of primary energy but two candidates, C_{50}^{250} the integral of the amount of light between 50 and 250m and $\emptyset(200)$, the Cerenkov light flux at 200m will be considered in this particular work. Data used for this interpretation of the analysis of the particle detector experiment were confined to those showers in which at least six Cerenkov light detectors had responded to give redundancy and reliability of shower record and those where the time and area fits were within acceptable limits. A discussion of the effects of those limits is beyond the scope of this thesis. It is not expected that large changes will occur in the time delay interpretation because of changes in the shower analyses resulting from later, more thorough analyses. Consideration of the many recorded showers with less than six detector responses will much increase the available data set (Walley, private comm. 1980).

The particular work referred to in this thesis deals with the response of two particle detectors, one located adjacent to Cerenkov

detector 1 and the other located adjacent to Cerenkov detector 6, see Figure 3.1. Particle detector 1, being at the centre of the array had the most frequent response providing the largest data sample. It recorded showers up to a core distance of 180 m with most showers falling in the 50 - 100 m range. The data from particle detector 6 was added to extend the range of investigation out to $\sim$ 250m from the core, since recorded showers were usually at > 150m core distance from detector 6.

In all, 131 measurements of the particle density and time data were made at core distances from 32 m to 317 m in 94 showers incident at zenith angles $\lesssim 50^{\circ}$ of primary energy estimated to be 10^{16} - 10^{17} eV.

CHAPTER 4

RESULTS

4.1 Introduction

The aim of this work is to refine our understanding of the time delay between the Cerenkov light and the particles in large air showers. We hope this measurement may yield a shower parameter which is sensitive to cascade development. The present work follows up the work done at Haverah Park (Shearer 1978) and the earlier work from the Dugway Experiment (Chantler et al. (1979)).

The lateral distribution of the time delay will be presented for showers recorded in three different zenith angle ranges, 0° - 34°, 34° - 44° and 44° - 51°. The ranges of 0 - 0.2, 0.2 - 0.4 and 0.4 - 0.6 in (sec θ - 1) corresponds to incremental increases of 172 g cm^{-2} in atmospheric depth between the observer and a fixed shower cascade maximum.

The results presented here are from 131 responses of the Cerenkov light and particle detectors at sites 1 and 6 in the large array (see Figure 3.1) and were obtained between 14 October 1979 and 19 November 1979.

Preliminary results are also presented for the particle density measurements made using detector 1. In addition to the measurement of the average lateral structure function for charged particles recorded in showers selected using the Cerenkov light detector array. The particle density measurements have contributed to our understanding of the best estimate of primary energy available from the Cerenkov light measurements. It is shown that the original energy estimator, $\emptyset(200)$ - the Cerenkov light at a core distance of 200 m - may be preferred to C_{50}^{250} - the integral of the Cerenkov light between 50 and 250 m core distance - which has been suggested recently by Shearer (1980).

4.2 The time delay results

The time delay between the Cerenkov light and the particles shows an increase with core distance. The earlier work, based on measurements between 50 - 125 metres, demonstrated this increase but the form of the increase could not be accurately observed. The present results covered a wider range of core distance and could not be satisfactorily fitted with a linear function of core distance.

An adequate fit was available using a relation of the form:-

$$TD = ar^n$$ where n is approximately equal to 2, and

TD is in nanoseconds and core distance, r, in metres.

The equations of the three curves for core distances greater than 50 m are:-

for the 0° - 34° range $\quad TD = 5.35 \times 10^{-5} r^{2.47}$ (ns)

for the 34°- 44° range $\quad TD = 1.30 \times 10^{-4} r^{2.36}$ (ns)

for the 44°- 51° range $\quad TD = 1.10 \times 10^{-3} r^{1.98}$ (ns)

The experimental data and these fits are shown in Figure 4.1.

The expected form of the relation and its sensitivity to zenith angle is not known from previous work or simulations and depends very much on the particular experimental system.

It would have been reasonable to have expected that the exponent of r may increase with zenith angle to allow the three curves to diverge at large core distances. The decrease of the exponent for inclined showers can be explained by considering how the time delay originates. In near vertical showers (0° - 34°) the time delay is the difference between a highly curved light front and a flat particle front. At the other extreme in inclined showers (44° - 51°) the time delay is the difference between a relatively flat light front and the flat particle front. It can now be seen that the time delay produced by the former case may be more curved than that produced by

FIGURE 4.1   Lateral distributions of the time
delay for the three zenith angle ranges.
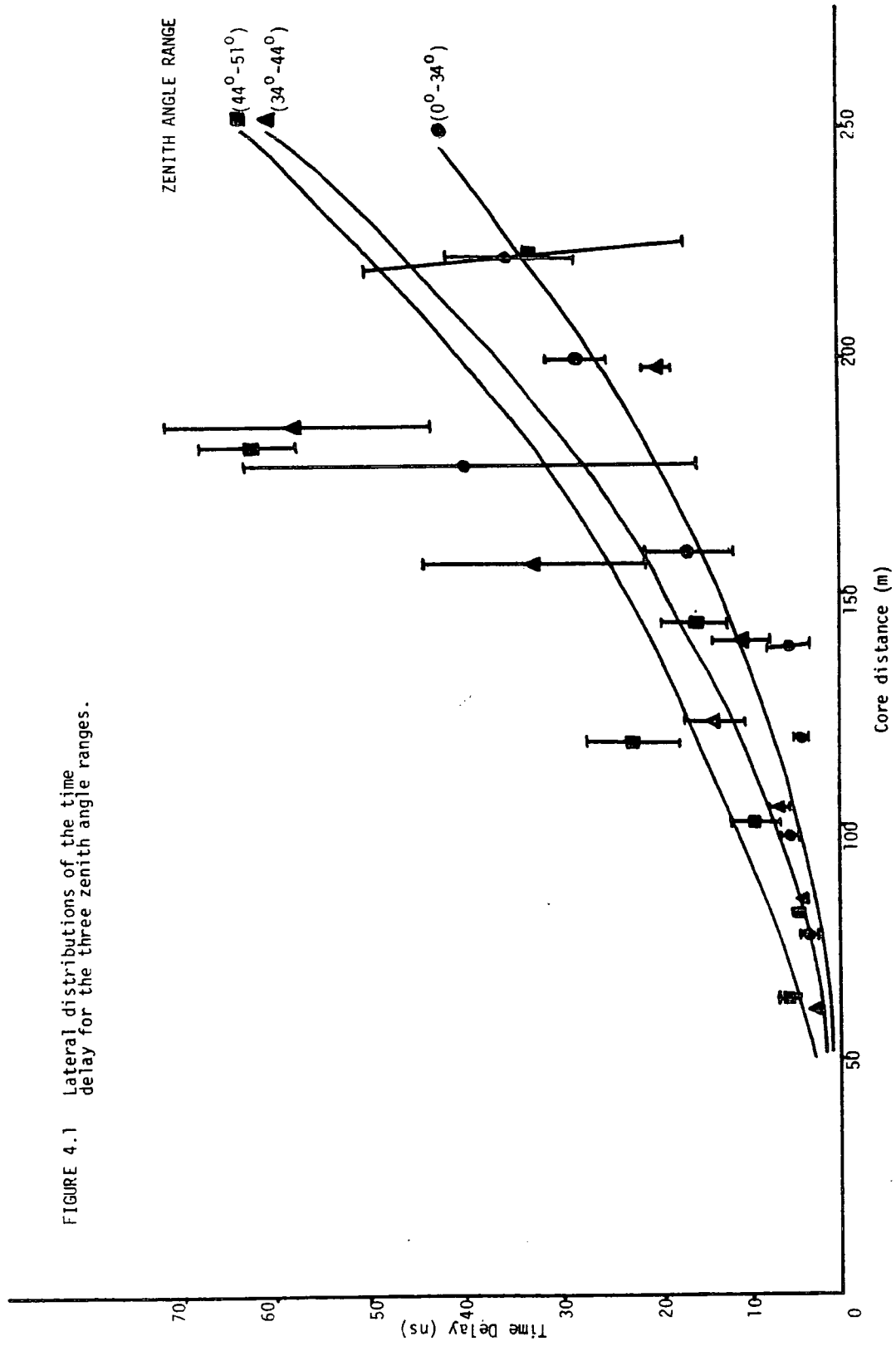
the latter case, hence the possible decrease of exponent with zenith angle. The complex nature of the problem is also demonstrated by this example. The time delay around 180 m core distance for all three zenith angle ranges seems high. Whether this is a statistical effect due to a shortage of data around this core distance or whether the time delay vs core distance relation is more complex than a power law will become evident when additional data are added in work to follow; (the data set will be more than doubled in work which continues on the interpretation of the Dugway Experiment - Walley, private communication 1980).

The lateral distribution of the time delay is shown here commencing at a core distance of 50 metres. Inside this distance the behaviour of the time delay has been seen to be complex and suggests an increase to 10's of nanoseconds on axis. No systematic attempt has been made here to investigate the time delay inside 50 m core distance, although the obvious explanation - core mislocation - is not thought to be appropriate.

If the time delay, at a fixed core distance in the range 50 - 250 m is considered for the three zenith angle ranges, we obtain the data of Figure 4.2.

The results can be understood if the distance between the observer and the depth of maximum electron development increases (with increasing zenith angle)the time delay increases for all distances 50 - 250 m.

However, in view of the complex nature of the time delay it may be premature to attach the obvious quantitative interpretation to the data of Figure 4.2, (i.e. the time delay at say 150 m changes by $\sim$ 1 ns per 30 g cm^{-2} change in depth of maximum).

4.3 The particle density results

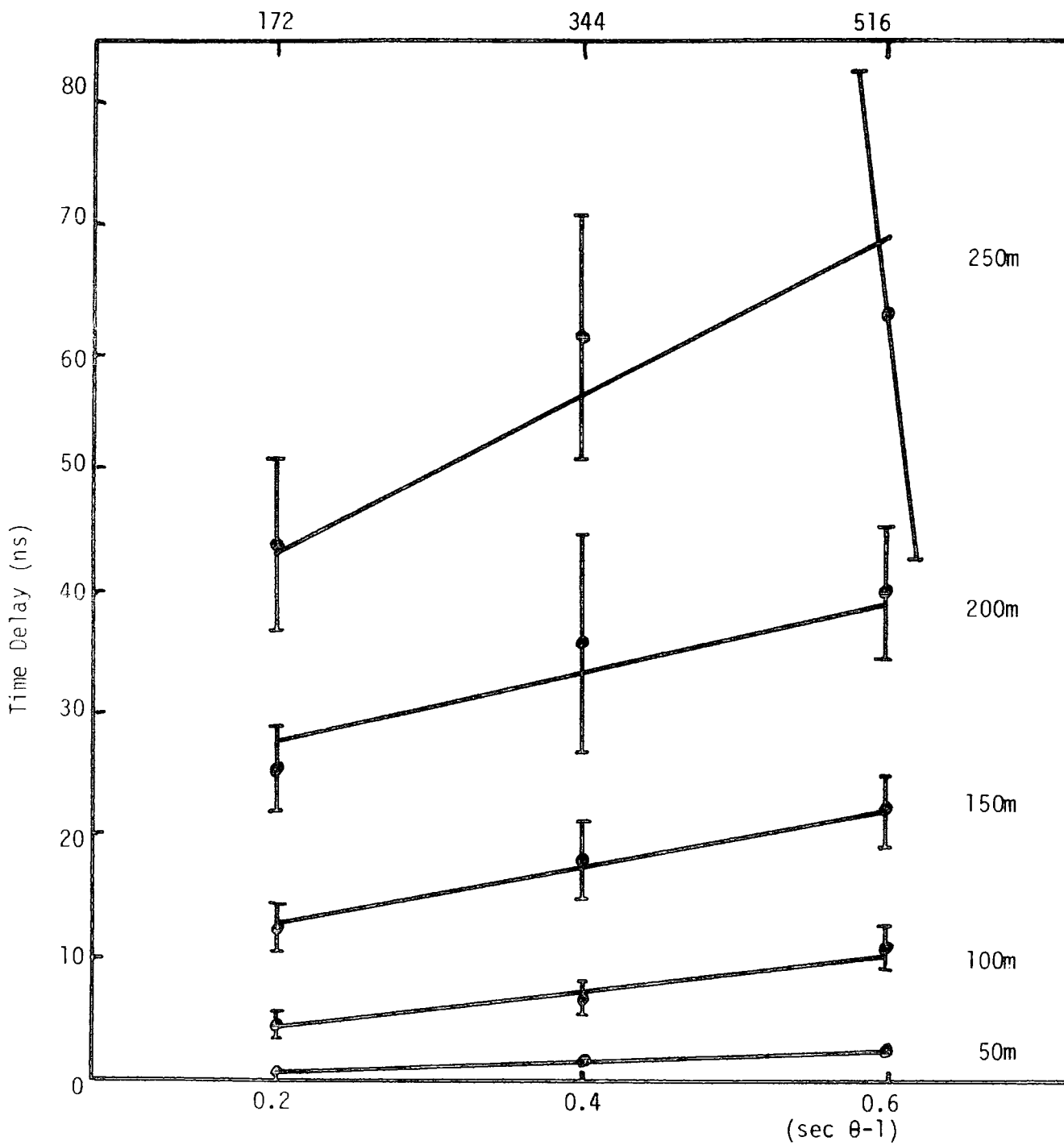An extensive air shower caused by a high energy primary yields

Figure 4.2   The time delay at fixed core distances for the three
zenith angle ranges.

more electrons at the observational level than one caused by a primary of lower energy. Also, a shower caused by a primary of fixed energy will contain more electrons near sea level if it develops later in the atmosphere, than if it develops higher than average.

In order to investigate the lateral distribution of the electrons allowance must first be made for the primary energy of the shower. The obvious method would be to divide the electron density measurement by the energy of the primary particle, if it were known. In effect this is what was done in the present work. Two different candidates for primary energy estimators, $\emptyset(200)$ and C_{50}^{250} have been used.

Figure 4.3 shows the relationship between the particle density measurements in showers from three zenith angle ranges normalised using the value for C_{50}^{250} in individual showers and core distance. Exponential forms for the fall off of density with core distance were the best fit to all the data points. It is noted that the three curves are very close to each other, i.e. the zenith angle has little effect. This may be interpreted as due to the fluctuation of the quantity C_{50}^{250} from shower to shower in a way which is similar to that of the electron number. (Primary energy estimators should show the opposite effect - i.e. independence of cascade development and reflect only the primary energy).

When the particle density measurements were normalised using the alternate energy estimator $\emptyset(200)$ and plotted against core distance, a much clearer picture of the lateral distribution of the electrons emerges - see Figure 4.4. As in the previous figure exponential structure functions were the best fit to the data points. The curves in Figure 4.4. are more widely spaced, showing some sensitivity to the longitudinal cascade (as shown by change in zenith angle) and

The lateral distribution of the particle densities normalized using C_{50}^{250} for the three zenith angle ranges.

Figure 4.3

$D = 27.9 \exp(-0.013r) \quad \theta(34\text{-}44^o)$

$D = 25.9 \exp(-0.012r) \quad \theta(0\text{-}34^o)$

$D = 25.9 \exp(-0.13r) \quad \theta(44\text{-}51^o)$

Normalized Density (C_{50}^{250})

R(m)
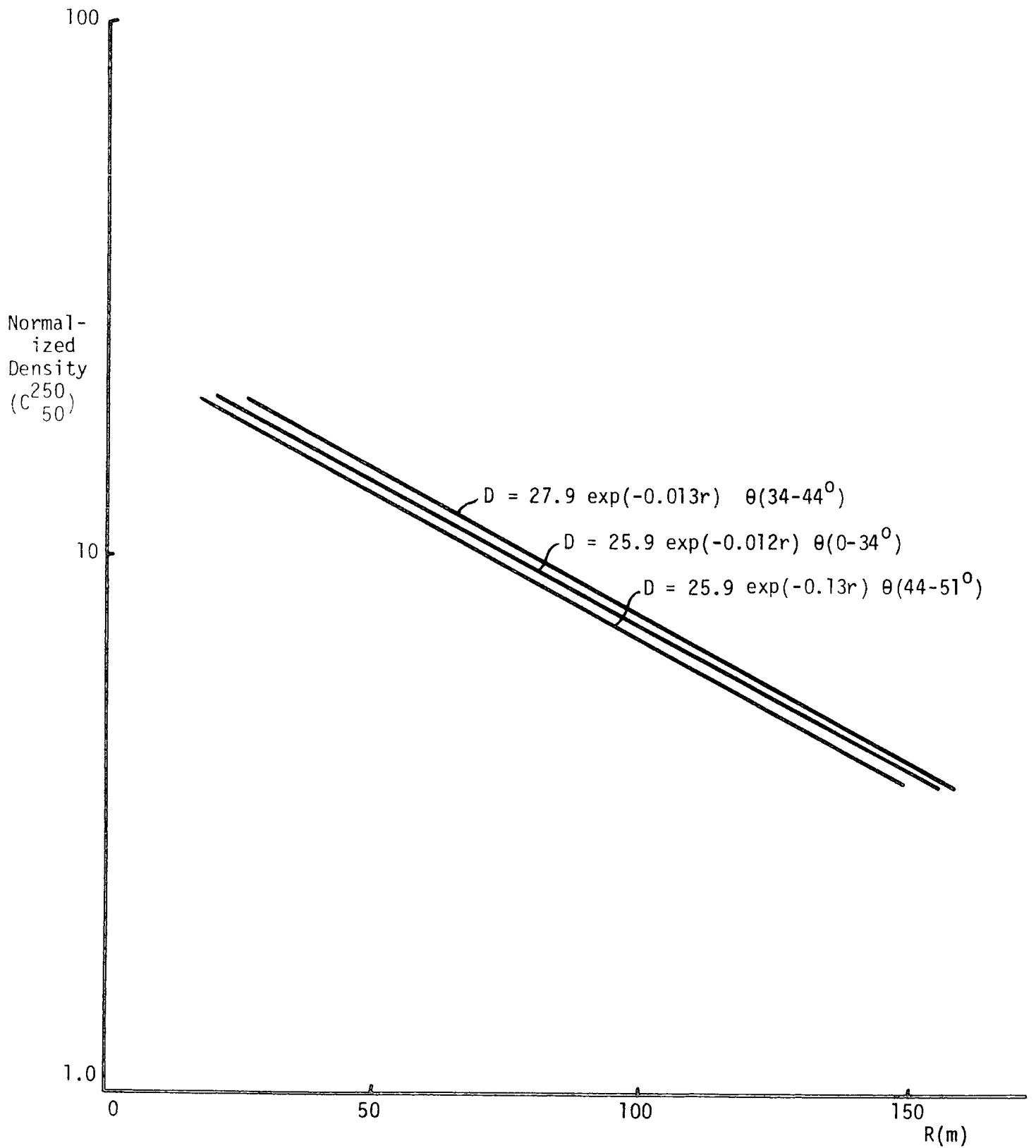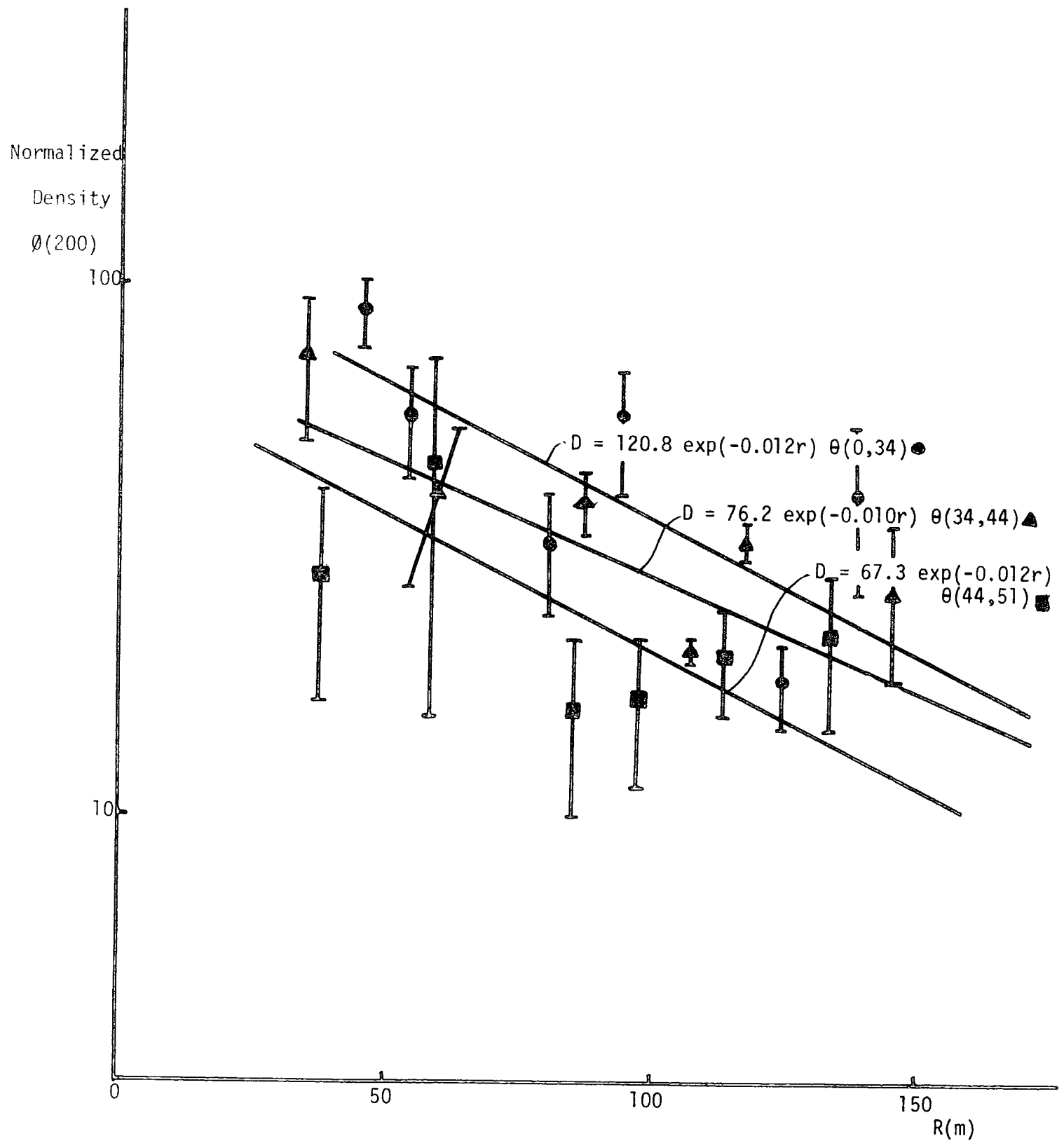
Figure 4.4   The lateral distribution of the particle densities
normalized using Ø(200) for the three zenith angle ranges.

hence presenting $\emptyset(200)$ as a more suitable primary energy estimator than c^{250}_{50}.

The ratio of the number of electrons to the number of photons incident at detector 1 at a particular core distance, here assumed to be 100 m, essentially the ratio $\dfrac{A1\ (100\ m)}{\emptyset(r)}$, is shown plotted against core distance in Figure 4.5. The behaviour of this ratio with zenith angle is interesting. For core distances < 90 m the ratio is larger, the greater the zenith angle; for distances > 140 m the ratio is smaller for the showers recorded at the larger zenith angles. The figure shows that for distances 110 - 120 m, the ratio varies little with zenith angle (and hence cascade development) i.e. the fluctuating electron density is followed by a similarly fluctuating photon density. The integral c^{250}_{50} is much influenced by the photon density at the distance 100 m and would also be expected to give a ratio $\dfrac{A1\ (100\ m)}{c^{250}_{50}}$ varying little with zenith angle. However, for distances approaching 200 m, the ratio $\dfrac{A1\ (100\ m)}{\emptyset(200\ m)}$ shows a clear sensitivity to zenith angle. Showers incident from near the zenith have large electron/photon ratios whilst the ratio of the electron integral to the 200 m photon signal decreases as the zenith angle increases. We thus suggest that the ratio $\dfrac{A1\ (100\ m)}{\emptyset\ (200\ m)}$ is a worthwhile development sensitive measure which can be considered similar to, in a simplified picture, the ratio $\dfrac{Ne}{N\gamma}$. Such a ratio is the classic case of the ratio of a development sensitive measure (Ne) divided by a primary energy estimator (Nγ - the penetrating Cerenkov light total flux).

Figure 4.5 The ratio of the number of electrons to the number of photons incident at detector 1 at a core distance range of 80 - 170 metres
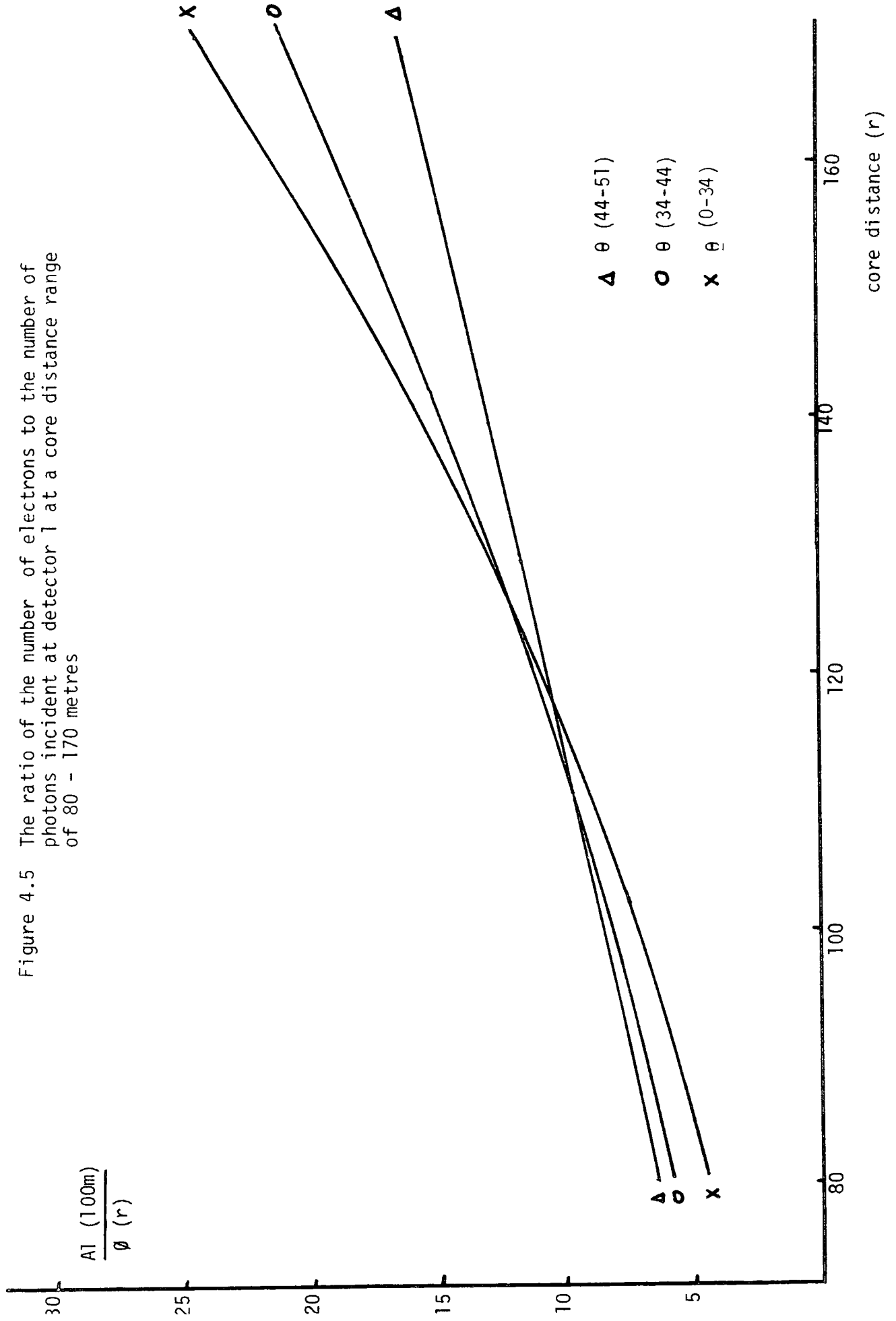
CHAPTER 5

CONCLUSIONS AND FUTURE WORK

5.1 Introduction

This study of the time delay between the particle front and the Cerenkov light front has been successful in the respect that a better measuring and recording system coupled with a higher event rate has resulted in a larger data set than was previously available. The previous work on the time delay suffered from poor statistics because of a low event rate combined with a much less effective data recording system. However, the experience gained from the earlier work provided great advances in our understanding of the time delay and these will be described in the sections to follow; several areas where further analysis of the new data is needed to establish fully the time delay as a fluctuation sensitive measure are also discussed.

5.2 The time delay between the particle and light fronts.

5.2.1 The form of the relationship between the time delay and core distance.

Over the core distance range 50 to 250 + m, a satisfactory fit to the present data was obtained using a power law relation between time delay and core distance with an exponent of approximately 2. The core distance range studied here was greater than in any previous work and it was no surprise to find that a more complicated form of structure function was necessary to fit the data than the linear fit which adequately represented the earlier data (see e.g. Chantler et al (1979)).

The detailed form of the relationship may well become more apparent in work to follow when the size of the data set is further increased (Walley (1981)).

5.2.2 The zenith angle sensitivity of the time delay.

A zenith angle sensitivity of the time delay structure function has been clearly demonstrated indicating that as the distance between the observer and the cascade maximum increases so also does the time delay, for all core distances. This forms the basis for the use of the time delay as a measure of the depth of maximum, since the variation with zenith angle is the clearest indication of a sensitivity to depth of maximum. In this respect, these time delay measurements have been very successful in indicating for the first time, changes in depth of maximum arising from changes in zenith angle. The observed zenith angle sensitivity of the time delay suggests a sensitivity, at a core distance of ~ 100m, to the change of depth of maximum of ~ 1 ns per 100 g cm^{-2}.

5.2.3 The primary energy sensitivity.

In the analysis to date, the time delay has not been shown to be sensitive to primary energy. At the present state of the data analysis this is not surprising because there may be substantial core mislocation errors left in the EAS data, (it should be remembered, the core analysis employed here is a preliminary one) there is also the fairly strong sensitivity to zenith angle and so within each zenith angle range the sensitivity to primary energy may well be masked. If the zenith angle contribution to the variation of time delay could be reliably removed, a fluctuation sensitive to the primary energy could be expected of the magnitude of ~ 5 - 10 ns per decade at $r \approx 150$ metres.

5.2.4 Future Work.

There is a need to extend the data to include at least three time delay measurements within a single shower as opposed to the one or two that form the basis of this work. This has already been achieved (Walley (1981)) and enables the form of the structure function of the time delay to be determined within an individual shower. Having obtained this, the time delay at 100m core distance can be interpolated (with no assumptions)

and may well be a valuable fluctuation-sensitive measure. Indeed, this quantity has already been seen to correlate well with the depth of maximum sensitive measure η (the Cerenkov light lateral distribution function exponent) (Walley - private communication). The steep showers (having high values of η) that develop deep in the atmosphere should, and indeed do, have small values for the time delay; conversely showers with a broad spread of the Cerenkov light which develop high in the atmosphere have large values for the time delay.

5.3 Particle density measurements using the plastic scintillator
      detectors.

There is an important requirement for a primary energy estimator in any EAS experiment. This is so because, to a first approximation, the observed particle density at a given core distance depends on the primary energy, the form of the lateral distribution of the particles, and the zenith angle of incidence. True fluctuations arising from cascade development differences, cause changes in particle density which are less than those from the three previous causes. In this sense the particle density is a less desirable cascade development measure than the time delay (which has no first order dependence on primary energy).

The problem of finding a primary energy estimator applies to all shower arrays. At Haverah Park, ρ(500) (the deep water detector response at 500 m core distance) was used on the strength of computer simulation results.

In other shower arrays the maximum number of electrons observed was used if they could be estimated eg Volcano Ranch. These are all quantities which for various reasons are thought to be the best primary energy estimator available although none are proven to be so. The same applies to the Cerenkov light density at 200 m ($\emptyset$(200)) used at Dugway, it has been shown in separate previous experiments to link with ρ(500) and maximum electron number. Until a better primary energy estimator is

found we must use the one we have most confidence in - for Dugway this is $\emptyset(200)$.

The lateral distribution of particles has been shown to have an exponential fall off with core distance and a zenith angle dependence indicating that inclined showers are older showers having less particles for a given primary energy (estimated from the amount of penetrating Cerenkov light). Future work should include particle density measurements with at least three detectors within an individual shower. This will enable the shape of the structure function to be determined (without any normalization requiring an accurate energy estimator). The shape of the structure function having been so obtained could be represented by an exponential function. The function parameter should then be shown to fluctuate with the Cerenkov light structure function, η. The number of particles per(Cerenkov light) energy estimator should also be shown to vary with η. The shape of the lateral distribution of particles and the ratio of the number of particles to the primary energy estimator may firstly be shown to be sensitive to zenith angle and hence large changes in the depth of maximum. It may also be possible to use the time delay measurements to verify that the particle density measurements are working as a fluctuation sensitive measure.

5.4 The smaller EAS arrays at Dugway.

All the data reported so far have been recorded using the large (400m) array. As the array dimensions were reduced the mean energy of the showers detected decreased and the showers had an increased probability of being incident from close to the zenith.

One of the most important potential developments of the time delay measuring technique is in showers of lower primary energy because these showers develop earlier in the atmosphere and reach their maximum electron density further away from the observation level.

Therefore, the time delay is inherently larger than showers initiated

by a high energy primary. This is in contrast to many measurements, for example the measurements of the Cerenkov light pulse which gets narrower as the energy of the primary decreases. Since the time delay increases, it is potentially a more readily measurable and stronger indicator of fluctuations in the smaller showers. This has been one of the long term aims of the time delay technique and present indications are that it may well be successful in the near future.

5.5 Summary

This work has established an improved relationship involving the time delay between the particle and light front, and core distance and shown the time delay to be sensitive to the depth of maximum electron development. The time delay measuring technique awaits full exploitation in work to follow on smaller showers of energy $> 5 \times 10^{15}$ eV. The electron density measurements, although secondary to the time delay estimators, also show potential as a source of at least one measure of the cascade development (the shape of the particle structure function) and perhaps two measures (the structure function shape and the ratio of the number of particles to Cerenkov light content (primary energy)).

ACKNOWLEDGEMENTS

REFERENCES

BERGESON, H.E., BOONE, J.C., and CASSIDAY, G.L., (1975), Proc. 14th
Int. Conf. Cosmic Rays, Munich, 8, 3059.

BLACKETT, P.M.S., Emission Spectra of the Night Sky and Aurora, Dep.
Gassiot Comm. of the Roy. Soc., (1948), p.34.

BOLEY, F.I., BAUM, J.H., PASLEDGE, J.A., and PEREVE, J.H., Phys. Rev.,
124, 1205 (1961).

BOLEY, F.I., (1964), Rev. Mod. Phys., 36, 792.

BRADLEY, E.F., and PORTER, N.A., (1960), Phil. Mag., 5, 305.

CERENKOV, P.A., Dokl. Akad. Nauk., SSSR, 2, 451, (1934).

CHANTLER, M., ORFORD, K.J., SHEARER, J.A.L., TURVER, K.E., and WALLEY,
G.M., (1979), Proc. 16th Int. Conf. Cosmic Rays,
Kyoto, 9, 42.

CHANTLER, M., McCOMB, T.J.L., ORFORD, K.J., SHEARER, J.A.L., TURVER, K.E.,
and WALLEY, G.M., (1979), Proc. 16th Int. Conf. Cosmic
Rays, Kyoto, 9, 56 .

DYAKONOV, M.N., KOLOSOV, V.A., KRASILNIKOV, D.D., KULAKOVSKAYA, V.P.,
LISCHENJUK, F.F., ORLOV, V.A., and SLEPTOV, I.Ye., (1973)
Proc. 13th Int. Conf. Cosmic Rays, Denver, 4, 2384.

DYAKONOV, M.N., KNURENKO, S.P., KOLOSOV, V.A., KRASILNIKOV, D.D.,
KULAKOVSKAYA, V.P., KUZMIN, A.I., ORLOV, V.A., SLEPTOV,
I.Ye., YEFIMOV, N.N., and YEGOROV, T.A., (1973), Proc.
13th Int. Conf. Cosmic Rays, Denver, 4, 2389.

ELTERMAN, L., (1968), Air Force Cambridge Res. Labs., Ref. AFC RL-68-0153.

ENCYCLOPAEDIA BRITANNICA, Vol. 5, p.200.

FRANK, I.M., and TAMM, I.G., Dokl. Akad. Nauk., SSSR., 14, 109, (1937).

GALBRAITH, W., and JELLEY, J.V., (1955), J. Atmos. and Terrestrial Phys.,
6, 250, 304.

GUZHAVIN, V.V., IVANENKO, I.P., MAKAROV, V.V, and ROGANOV, T.M., (1975),
Proc. 14th Int. Conf. Cosmic Rays, Munich, 8, 3029.

HAMMOND, K.T., ORFORD, K.J., PROTHEROE, R.J., SHEARER, J.A.L., TURVER, K.E., WADDOUP, W.D., and WELLBY, D.W., (1978), Il Nuovo Cimento, 1C, 315.

HESS, V.F., (1912), Phys. Z13, 1084.

JELLEY, J.V., and GALBRAITH, W., Phil. Mag., 44, 619, (1953).

JELLEY, J.V., (1967), Prof. in Cosmic Rays Phys., 9, 41.

KRIEGER, A.S., and BRADT, H.V., (1969), Phys. Rev., 185, 1629.

MALHOTRA, P.K., SHULKA, P.G., STEPHENS, S.A., VIJAYALAKOHMI, B., BOULT, J., BOWLER, M.G., CLAPHAM, V.M., FOWLER, P.H., HACKFORTH, H.L., KEEREETAREEP, J., and TOVEY, S.N., (1966), Nature, 209, 2567.

MALOS, J.D., (1955), Ph.D. Thesis, University of Sydney.

MALOS, J.D., MILLAR, D.D., and WALLACE, C.S., Journ. Phys. Soc. Japan, Suppl., A-III, 114, (1962).

McCUSKER, C.B.A., (1967), Proc. 10th Int. Conf. in Cosmic Rays, 5397.

PROTHEROE, R.J., (1978), Ph.D. Thesis, University of Durham.

SHEARER, J.A.L., (1978), M.Sc. Thesis, University of Durham.

SHEARER, J.A.L., (1980), Ph.D. Thesis, University of Durham.

TURVER, K.E., (1963), Ph.D. Thesis, University of Leeds.

WALLEY, G.M., (1981), Ph.D. Thesis, University of Durham, in preparation.

WELLBY, D.W., (1978), Ph.D. Thesis, University of Durham.